A Physical and Numerical Model Investigation of a River Flow Diversion and Assessment of Large Woody Debris Types

Brian Perry

Thesis submitted to the University of Ottawa in partial fulfillment of the requirements for the degree of

Master of Applied Science in Civil Engineering

University of Ottawa

Faculty of Engineering

Department of Civil Engineering

Acknowledgements

I would like to thank my supervisor Dr. Colin Rennie, without whom I would have not been able to complete this thesis nor would I have sought out a Masters degree in Water Resource Engineering. It was in my 3rd year of university that I was fortunate enough to have him as a professor for hydraulics. It was a challenging course and yet I found it to be one of the few courses that year for which I was passionate. A year later, during our capstone project, I was again partnered with Dr. Rennie and gained valuable experience in the fields of numerical and physical modelling. Upon completion of this project and my undergraduate degree, he was kind enough to offer me the opportunity to continue my education on what he called a very exciting project. I happily accepted knowing that this was a once in a lifetime opportunity and so for that I am ever grateful.

I would like to thank my co-supervisor Dr. Andrew Cornett, Paul Knox, Mitch Provan and the NRC-OCRE division as a whole for the experience and all the lessons they taught me. The 6 months I spent working in tandem with all of the excellent people there will not be forgetting nor taken for granted.

I would like to thank my friends and family who have supported me through my entire life and especially in the past 7 years of academia. More specifically I would like to thank my mom, Janice, my father, Bruce and my two sisters, Nicole and Jeanelle, who were always there for me in every decision I made.

I am truly grateful for the opportunities I was presented and hope that I can continue to grow as an academic and person in a way that everyone who I have listed above, who I deeply respect, can be proud of.

Abstract

The extreme flooding event that occurred in 2013 in Alberta, Canada was at time the most costly natural hazard event in the nation's history with damages exceeding $5 billion. Due to this event, an increased effort for flood mitigation strategies began and resulted in the proposal of the Springbank Off-Stream Storage Reservoir to divert and detain Elbow River flow upstream of the City of Calgary. In order to validate the design of the flow diversion structures, a large (1:16) scale physical model was constructed. The model tested among other things, the impact of large woody debris (LWD) on the flow diversion structures. The LWD modelling included a comparison of LWD manufactured from smooth cylindrical dowels versus natural tree limbs of the same dimensions. The results from the physical model led to a series of design changes for the diversion structures that likely would not have been identified without physical modelling. The LWD material comparison demonstrated significantly different behaviours between LWD types. Specifically, LWD manufactured from natural tree limbs was significantly more likely to accumulate in debris dams on the diversion structures. The impact of root wad was also investigated and proved to play a major role in the damming characteristics and blocking probability of debris. Following the physical model investigations, a numerical simulation was completed in order to examine further the hydrodynamic results obtained from the Springbank project. Using TELEMAC MASCARET's open source free surface flow program TELEMAC 2D, a two dimensional simulation was completed using data from the physical model. Flowrates and velocities from both models were compared and discrepancies between the two are identified. Reasoning for these differences as well as future works for the numerical model are presented.

Table of Contents

Acknowledgements ii

Abstract iii

List of Figures vi

List of Tables viii

List of Symbols ix

1.0 Introduction 1

1.1 Organization of Thesis 2

1.2 Literature Review 2

1.2.1 Large Wood and Recruitment into the River Corridor 2

1.2.2 Flooding and Impact of LW 3

1.2.3 Debris Racks and Damming Process 4

1.2.4 Modelling of LW 5

1.3 Research Objectives 7

1.4 Novelty of Study 7

1.5 Project Contributors 8

2.0 Investigation of Large Woody Debris Impact on Structures and Debris Type Comparison in a Large Scale Physical Model 9

2.1 Introduction 9

2.2 Physical Model 11

2.2.1 Initial Design 12

2.2.2 Modified Design 13

2.2.3 Debris Barrier 14

2.3 Large Woody Debris 14

2.4 Testing Method 15

2.4.1 Debris Raft Testing 16

2.4.2 Repeatability Testing 16

2.4.3 Single Debris Testing 16

2.4.4 Debris Jamming Classification 17

2.4.5 Time-lapse Photo Analysis 17
2.5 Results 17
2.6 Discussion 22
2.6.1 Performance Assessment & Debris Structures 22
2.6.2 Debris Type Comparison 23
2.6.3 Impact of Root Wad 23
2.6.4 Angle of Approach 24
2.6.5 Debris Dam Characteristics 25
2.6.6 Scaling of Large Woody Debris 25
2.7 Conclusion 26
3.0 Numerical Model 27
3.1 Introduction 27
3.1.1 Program Selection 28
3.2.1 Model Domain 28
3.2.2 Model Data 29
3.3 Model Parameters 32
3.3.1 Mesh Generation 32
3.3.2 Boundary Conditions: Model Inputs, Outputs and Control Sections 33
3.3.3 Simulation Parameters 35
3.3.4 Model Calibration 36
3.4 Results 36
3.5 Discussion 41
3.5.1 Model Limitations 45
3.6 Conclusion 45
4.0 Thesis Conclusions 47
5.0 Recommendations for Future Work 48
6.0 References 50
Appendix A: Debris Orientation Angles and Dam Outlines 54
Appendix B: Physical Model Construction 62
Appendix C: Drogue Paths 68

List of Figures

Figure 1: Overview of Springbank Project, outlining locations for flow structures and storage reservoir along the Elbow River upstream of the City of Calgary 11
Figure 2: Plan view of the original structural design, with the diversion structure leading left and the main channel leading right. The 7 release locations for debris testing are identified upstream of the structures. 13
Figure 3: Modified Diversion and Spillway (Main Channel) Structure 14
Figure 4: Root Wad attached to LWD (left), debris fabrication at NRC facilities (right) 15
Figure 5: 17 piece dam jammed due to root wad (left) 38 dam jammed due to debris roughness (right) with no debris rack in place 19
Figure 6: Repeatability Results: The largest/single box represents the median to the 75th percentile (Q3) of the data and the smaller box represents the 25th percentile (Q1) to the median (MD only). The whiskers are equal to 1.5 times the difference between Q3 and Q1. 19
Figure 7: MD (left) and RDR (right) angle of arrival with pieces greater than one standard of deviation from the mean highlighted in yellow 21
Figure 8: Outline of single debris test dam (left) and a 10-piece dam (right) for all debris types. MD yellow, RDN green and RDR red. 21
Figure 9: Drogue Paths for 760m^3/s flow condition 27
Figure 10: Springbank physical model layout with area to be modelled numerically outlined in red (NRC, 2016) 29
Figure 11: Water levels (m in prototype scale) for diversion and main channel (WP11) weirs from the physical model during the 760 m^3/s scenario for 600s time interval 30
Figure 12: Flowrates (m^3/s prototype scale) for diversion and main channel weirs from the physical model during the 760 m^3/s scenario for 600s time interval 30
Figure 13: velocity data (m/s prototype scale) for ADV locations 1, 2, 6 from the physical model during the 760 m^3/s scenario for 600s time interval 31
Figure 14: 3D view of the Springbank mesh used in numerical modelling 32
Figure 15: 2D view of numerical model mesh with control sections (black), input (left), outputs (right) in red and ADV locations (purple). The provided scale is in meters and represents the elevation of each node. 34
Figure 16: variable bottom roughness for numerical model with forested regions (blue) 35
Figure 17: Flowrate through Diversion (Blue) and Main (Orange) channel control section 37

Figure 18: numerical simulation velocities in m/s at 0 (top) and 60 (bottom) minutes 38
Figure 19: simulated drogue paths overlaid onto velocity results at 60 minute time step. Numerical drogues represented as squares and physical drogues represented as X's. The velocity colour scale is the same as in Figure 18. 39
Figure 20: Drogue paths for main and secondary upstream channel. Squares (Numerical) and X's (Physical) represent the drogue at each time step. The velocity colour scale is the same as figure 18. 40
Figure 21: Drogue paths for floodplain. Squares (Numerical) and X's (Physical) represent the drogue at each time step. The velocity colour scale is the same as figure 18. 40
Figure 22: Scalar flowrate at 60 minute time step (m^2/s) 41
Figure 23: Drogue paths at confluence from physical model at 760m^3/s flow condition 44
Figure 24: Angle of Departure for MD 54
Figure 25: Angle of Departure for RDN 54
Figure 26: Angle of Departure for RDR 55
Figure 27: Angle of Arrival for RDN, Debris outside of one standard deviation of the mean highlighted in yellow 55
Figure 28: 9 piece dam for MD 56
Figure 29: 10 piece dam for MD 56
Figure 30: 9 piece dam for RDN: 1 (red), 2 (yellow), 3 (green) of 3 dams 57
Figure 31: 10 piece dam for RDN: 1 (red), 2 (yellow), 3 (green) of 8 dams 57
Figure 32: 10 piece dam for RDN: 4 (red), 5 (yellow), 6 (green) of 8 dams 58
Figure 33: 10 piece dam for RDN: 7 (red), 8 (yellow) of 8 dams 58
Figure 34: 9 piece dam for RDR: 1 (red), 2 (yellow), 3 (green) of 6 dams 59
Figure 35: 9 piece dam for RDR: 4 (red), 5 (yellow), 6 (green) of 6 dams 59
Figure 36: 10 piece dam for RDR: 1 (red), 2 (yellow), 3 (green) of 8 dams 60
Figure 37: 10 piece dam for RDR: 4 (red), 5 (yellow), 6 (green) of 8 dams 60
Figure 38: 10 piece dam for RDR: 7 (red), 8 (yellow) of 8 dams 61
Figure 39: Template installation and backfilling with gravel (NRC, 2016) 62
Figure 40: Grout finishing and installation of scaled trees (NRC, 2016) 63
Figure 41: Continued construction of the Springbank model (NRC, 2016) 64
Figure 42: Installation of flow structures and retaining walls (NRC, 2016) 65
Figure 43: Finished flow structures with riprap placed directly upstream (NRC, 2016) 66

Figure 44: Completed model prior to testing with sampling equipment installed (NRC, 2016) 67
Figure 45: A_760_2: downstream drogue paths for 760m^3/s flow condition 68
Figure 46: A_760_4: upstream drogue paths for 760m^3/s flow condition 68
Figure 47: A_760_6: downstream drogue paths for 760m^3/s flow condition 69
Figure 48: A_760_7: downstream drogue paths for 760m^3/s flow condition 69

List of Tables

Table 1: Diversion and Main Channel Design and (model) Flowrates 12
Table 2: Large Woody Debris Characteristics 15
Table 3: Debris Raft Test Jamming Results for Manufactured Debris (MD), Realistic Debris without Root Wad (RDN) and Realistic Debris with Root Wad (RDR) 18
Table 4: Single Debris Test Results 20
Table 5: Angle of arrival and departure (from vertical) for single debris test (in degrees) 20
Table 6: 9 and 10 piece dam area statistics by debris type 22
Table 7: Single debris dam size and number of pieces 22
Table 8: Example Froude scaling of quantities 31
Table 9: Element properties for the numerical mesh generated in BlueKenue 33
Table 10: Prescribed Flowrates and Elevations for Numerical Model 34
Table 11: Summary of Diversion and Main Channel Flowrates 37
Table 12: mean velocity results for the physical (downscaled) and numerical model at probe locations 1, 2 & 6 38

List of Symbols

ΔS: Change in storage for a river section

Li: Lateral inputs to a river section

Lo: Lateral outputs from a river section

Qi: Fluvial inputs to a river section

Qo: Fluvial outputs from a river section

D: Rate of decay of large wood within a river section

Δt: Change in time for a river section

λ: Froude scaling criterion

Q: Flowrate, listed in m^3/s

V: velocity, listed in m/s

1.0 Introduction

During the summer of 2013, the city of Calgary experienced one of the most financially devastating floods in the history of Alberta with damages exceeding $5 billion (Cornett et al. 2017). The primary cause of this flooding was due to excess rainfall over a short period, resulting in the Elbow River exceeding its normal capacity of 180 m^3/s by a significant amount with flows of up to 1240m^3/s. In order to mitigate future flooding, the Province of Alberta in partner with Stantec Consulting Inc. proposed the Springbank Off-stream Storage Reservoir. The project would divert excess flow to a temporary storage reservoir located upstream of the City of Calgary along the Elbow River, maintaining normal flow conditions in the river. Following the flood event, the reservoir would release the temporarily stored water back into the river, mitigating potential flood damage (Knox, Cornett, and Provan 2016).

In order to validate the design of the diversion system, the National Research Council of Canada – Ocean Coastal and River Engineering (NRC – OCRE) research centre was subcontracted to create a physical model at the Ottawa Campus. Realizing the research opportunity, NRC OCRE then collaborated with the University of Ottawa department of Civil Engineering to develop a physical model and validate the design of the proposed Springbank project. Included in the design validation of the diversion system was an investigation of potential impacts from large woody debris (LWD). For the present thesis research, as part of this investigation an in-depth analysis was conducted of the influence of LWD characteristics on LWD behaviour in the physical model. Specifically, model LWD was manufactured from different materials, including cylindrical dowels, natural tree limbs, and natural tree limbs with an attached modelled root wad. The performance of these LWD types was investigated with respect to their interactions with the diversion structure, their damming mechanics, and their blocking probability.

The construction of the physical model took several months of full time work, and several more months were required for calibrating, testing, updating and re-testing the model once completed. The author worked in tandem with the NRC OCRE staff full time at all stages of the project to provide the clients with an optimal product. Upon completion of the client's task list, the author was given access to the model to complete his Master's research and was given access to all of the data accrued throughout earlier testing. Appendix B provides an in-depth description of the construction process for the physical model.

1.1 Organization of Thesis

This thesis is comprised of an original research article, presenting the novel findings of this Master's research, which is to be submitted to a peer-reviewed journal. The article presents a brief overview of current large wood research, and provides a description of the physical model constructed at the NRC-OCRE facilities, followed by the testing procedures and results from the LWD investigations, and a discussion of their importance and impacts on future physical modelling.

Complementing this article, Chapter 1 presents an extensive literature review of large wood and its impact on river systems including conceptual models for its entrainment, previous physical modelling experiments and field investigations. Chapter 2 presents the previously mentioned original research article entitled *"Investigation of Large Woody Debris Impact on Structures and Prototype Comparison in a Large Scale Physical Model"* written by the author of this thesis and edited by Dr. Colin Rennie and Dr. Andrew Cornett. Chapter 3 presents numerical modelling work completed in tandem with the physical modelling research, while Chapter 4 presents thesis conclusions and discusses potential future works as well as recommendations based on the research conducted for this thesis.

1.2 Literature Review

1.2.1 Large Wood and Recruitment into the River Corridor

Large wood (LW) is defined as pieces of wood that exceed 10 cm in diameter and 1 m in length. The impact of LW on rivers and the river corridor has been a topic of research for over 50 years (Wohl et al. 2016). Wood pieces that are present within the river corridor, which includes both the channel and active floodplain, have the potential to affect the bed morphology, water levels, sediment transport and many other properties of the system. For this reason, understanding the method in which LW enters the river corridor and its behaviour once entrained is vital. The recruitment of LW is a complex process but is eloquently explained via the wood budget, a conceptual model created to balance the inputs and outputs of LW through a section of a river system (Wohl 2017). The wood budget defines the storage (ΔS) as the sum of all LW entering and leaving the defined river section for a given period (Δt). Two types of inputs exist to the system, lateral inputs (Li) and fluvial inputs (Qi), while three outputs exist for the same system; lateral outputs (Lo), fluvial outputs (Qo) and decay (D).

$$\Delta S = (Li - Lo + \frac{Qi}{\Delta t} - \frac{Qo}{\Delta t} - D)\Delta t$$

Fluvial inputs and outputs are considered LW that is actively within the channel, being moved through the section due to flow; therefore, the fluvial inputs are dependent on the output of the section directly upstream. The fluvial inputs and outputs are impacted by LW mobility, which is dependent of the ratio between LW size and river width. Decay is the deterioration of any LW by the processes of abrasion or rot while in the river section. Lateral inputs and outputs focus on the corridor properties, more specifically the amount of downed LW within that section, the rate of bank or floodplain erosion as well as the impact of biota such as beaver adding or removing LW. These lateral inputs and outputs are very much dependent on the river corridor properties and geographic location and can be difficult to quantify; however, depending on the size of the river, they may account for a large portion or a fraction of the LW recruitment. Based on the above equation, it is apparent that small rivers in headwater areas will see the largest influence from lateral inputs and outputs, where little to no fluvial inputs/outputs exist. Further downstream, fluvial inputs and outputs tend to dominate, as these sections have greater flow and already mobile LW from the upstream sections.

1.2.2 Flooding and Impact of LW

Flood events are often correlated with an increase in LW recruitment and are often studied in tandem due to this (Davidson, MacKenzie, and Eaton 2015). Transport of LW is a natural process and occurs regardless of flood events, however in forested or partially forested catchments, flood events and their associated damage are exacerbated by the presence of LW (Steeb et al. 2017). Several factors contribute to this increase in risk when LW is present in a flooding event. Firstly, it increases flow resistance in the channel resulting in slowed flood flows and an increased likelihood of inundation (Steeb et al. 2017). It has the potential to block structures such as dams and bridges, which may lead to structural damage through increased scour (Pagliara and Carnacina 2010) or aggravated flooding due to increased water levels. It also has the potential to create unstable logjams, which if freed act as a large amount of material moving through the channel (Schmocker and Hager 2011). Lastly, LW can increase sediment deposition at critical locations (Steeb et al. 2017). These potentially devastating impacts of LW therefore make it pertinent to study the transport of LW in river systems and the impact that LW has on the river flow and morphology.

Investigating the impact of LW on flow resistance in a field study of small river channels, it was determined that there exists the potential for an increase flow resistance, expressed as Manning's n, of up to 40% (Abt, Dudley, and Fischenich 1998). Field studies for the Queets River demonstrate the extent to which LWD can affect channel morphology; it was noted that debris jams are capable of altering local

hydraulics and morphology for decades and potentially centuries while laboratory studies were able to accurately recreate these observations (Abbe and Montgomery 1996). Pool and bar formations were directly correlated to different debris jams proving the important role that LW plays in channel development. Continuing onto the impact of debris damming, many physical models have investigated the extent to which LW impacts scour on hydraulic structures such as bridge piers. Based on laboratory experiments, scour depths can be increased by up to three times normal scour depth when debris is accumulated on piers (Pagliara and Carnacina 2010).

1.2.3 Debris Racks and Damming Process

One strategy for mitigating the potential hazards from LW is to keep the debris upstream at key locations with the use of debris racks (Schmocker and Hager 2013). These racks, which are constructed of steel/concrete posts, are often placed directly in the river upstream of locations susceptible to damming and structure damage, such as bridges. The accumulation process at a debris rack begins with initial debris arriving at the rack followed by backwater rise due to the dam and increased damming to the point of a mobile debris carpet forming at the rack. The damming process upon debris racks is dependent on many factors, which are currently being investigated. (Schmocker and Hager 2011) found the blocking probability of debris on a bridge deck to be dependent on the relative size of the LW, the diameter of the root wad as well as the freeboard height for scenarios with a structure spanning the width of the channel. (Furlan et al. 2017) investigated the impacts of LW density on blocking for an Ogee Crest spillway and found that denser debris was more likely to block the spillway. (Ward E.Sanford, Gerolamo Casile 2015) observed that the irregularities in debris shape were impactful in the damming process, making it difficult for researchers to determine which parameter is most important in the damming process. All previous research, however, agrees that the damming process is in fact random and this must be considered when investigating LW damming.

For debris racks specifically, the span between piers plays a major role in damming and the ratio of mean debris length to rack opening is crucial. Design ratios recommend that the ratio of pier span and debris length be less than ½ to optimize debris trapping (Horiguchi et al. 2015). In order to determine these mean lengths, researchers rely heavily on field investigations. Following a LW event, measurements of the debris pieces found along the riverbanks are taken and their mean computed. This is an informative process and one of the few methods to obtain information regarding LW characteristics, but debris is likely to degrade during the damming process (Schmocker and Hager 2011)

and may not be truly indicative of actual debris properties. Therefore post-flood investigations can provide good insight as to the LW characteristics but are not definite (Kramer et al. 2015).

1.2.4 Modelling of LW

Fluvial hydraulics is a complex process in itself and the addition of LW adds an additional degree of complexity, making these systems extremely difficult to model numerically. Several modelling programs exist for simulating open flow in one, two and, three dimensions; however, modelling complex solids within these numerical models is currently being researched (Horiguchi et al. 2015). (Mazzorana et al. 2018) provides an in-depth review of recent approaches to modelling large-wood related hazards numerically. (Hafs et al. 2014) created a coupled hydrodynamic and bioenergetics model to determine the impact of LW on a river system with respects to growing juvenile chinook salmon but admitted that true validation of the LW scenarios were not possible due to the complexity of LW. The current approach for determining LW transport relies on computing the hydraulics of the river system in question and using these results to estimate the LW mobilization (Largiader 2011), yet no deterministic model for predicting LW transport in a short period of time exist to date (Villanueva, Prospective, and Engineering 2014). Additional numerical approaches exist such as the Iber-Wood model (Mazzorana et al. 2018) which is used for back analysis in partner with post-flood field investigations and was successful in recreating the deposition patterns of LW and areas of preferential log jam formation. This model shows the great potential of numerical models however, its calibration required post flood data. Direct observations of LW transport during floods is difficult to obtain and the data is scarce (Ravazzolo et al. 2017) and acts as an additional constraint to numerical modelling.

For this reason, physical modelling has become the standard for validating fluvial structure designs or investigating LW behavior. The goal of physical modelling focuses on recreating similar test conditions to those seen in the field within a controlled environment. This often results in creating scaled models due to laboratory constraints. The scaling criterion typically used in open flow models is Froude scaling, which assumes inertial and gravitational forces dominate in comparison to viscous forces (Cornett et al. 2017). Therefore, when selecting a model scale, it is important that the resulting dimensions of the model remain large enough that viscous forces will not begin to compete with gravity or inertia. Fortunately the scale at which this occurs is very small and it is not uncommon to see model scales within the 1:50 – 1:100 range (Rusyda 2015). At these ranges, however, due to the typical dimensions of a river cross section, the vertical dimensions of some models can become minute enough that viscous forces may be impactful. These conditions may lead to researchers using vertically distorted models in

order to adhere to their specific constraints. Distorted models offer a practical way to conduct physical modelling but one must consider the impact this distortion has, such as impact on velocity profile and vertical accelerations, and should find a compromise in a distortion factor that adequately models flow and abides by the area constraints (Ettema et al. 2007).

With respect to designing scaled LW to use within physical models, researchers have taken many approaches. Typically, geometric scaling is used; field investigations will provide the mean dimensions of the debris and the model scale will be used to reduce the model LW to the appropriate size to be used within the model (Schmocker and Hager 2013). Where variation occurs is the material selection as well as adherence to realistic debris shape. Smooth cylinders fabricated from PVC or wood have been used in many flume studies (Gallisdorfer et al. 2014) and at small scales these smooth cylinders may be considered adequate in terms of simulating the behavior of LW within a river system. Investigating the drag forces on smooth cylinders versus similar sized logs of both oak and hackberry, it was noted that the log roughness caused the model LW to behave similarly but not identically, meaning that smooth cylinders may not be a realistic representation of LW (Carlos V. Alonso, Shields, and Temple 2005). This drag force investigation did not consider the impact of root wad on the LW behavior, and root wad has been noted in field investigations following flood events on over 60% of debris pieces (Knox, Cornett, and Provan 2016). To address this, modelers have utilized strips of wood in an “X” pattern attached to the base of the tree stem (Welber, Bertoldi, and Tubino 2013), used additional wood pieces to simulate branches along the lower portion of the stem (Horiguchi et al. 2015), or simply used trunks/root wad harvested from natural resources (Schmocker and Hager 2011). Many of these improved large wood debris types however still use smooth cylinders to represent the stems, and therefore researchers are still divided on the optimal model large wood debris type design for testing LW.

In addition to model large wood debris type selection, researchers must be aware of scale effects within their model. One of the most notable and of concern when working with LW is the increased stability of the scaled debris. As noted by (Schmocker and Hager 2011) debris did not break or degrade during damming or when interacting with structures like it would in nature. An argument was made that due to the density of the debris dam, the debris would likely not break. However, if investigations are done upon single debris or loose dams, consideration should be given for the increased stability of model LW. Similarly, consideration must be given for the hydraulics of the model. Many experiments are conducted within flumes, which are often considered hydraulically smooth (Schmocker and Hager 2013), which is not the case in most rivers being modelled. Buoyancy and buoyancy depth plays a key role in LW

mobility in models (Welber, Bertoldi, and Tubino 2013), and as such density of scaled LW should also be considered in modelling.

1.3 Research Objectives

This study aims to improve the knowledge of large woody debris interactions with flow structures and to determine the impact that different large woody debris types currently used in physical modelling may have on the results obtained in these models. The Springbank project provides an opportunity for large scale physical modelling to be conducted in a non-flume environment with several different large wood debris types. By performing a comparative analysis of these different debris types, we can determine which debris types most accurately depict large wood in nature as well as determine the extent to which the performance of natural debris may differ from the performance of simplified debris used in research. Additionally, post processing of the results obtained in the model can be used to investigate the damming procedure of large wood at debris structures and the impact that orientation within the flow has on the dam formation.

1.4 Novelty of Study

Previous experiments involving large woody debris tend to focus on a single debris type, are limited in model scale, or are conducted in a flume. This study presented an opportunity for a comparison to be conducted between debris manufactured from natural resources versus similar debris manufactured from smooth cylindrical dowels. This direct comparison was deemed important as limited to no data are available concerning these two methods for creating large wood debris to be used in physical modelling. Additionally, the facilities utilized for the construction of the physical model are amongst the largest within North America, allowing for a larger model scale to be used (1:16) and in turn, larger debris. As scale-effects must always be considered when physical modelling, conducting investigations at scales approaching 1:1 allows these to be minimized. Based on the extensive literature review, the model scale used for these experiments is amongst the largest in a large wood debris physical model study, while no other non-flume based models were found to have larger scales. Lastly, the testing of the large wood debris was conducted in a spatially complex scaled 3D river section that included forested floodplain, not within a flume. This adds a layer of novelty to the experiment, as this exact model has never been investigated, and 3D flow conditions were studied that are not possible to evaluate within flume-based studies.

1.5 Project Contributors

The Springbank physical model was constructed at the NRC-OCRE facilities under the supervision of Dr. Andrew Cornett and Paul Knox by the author, Mitchel Provan, Alistair Rayner, Yvan Brunet, David Hnatiw, John Marquardt, Bill Gow, and Nathalie Brunette. The debris collection and construction was conducted by the author with assistance from Yvan Brunet. The debris testing presented in Chapter 2 was conceptualized by the author with assistance from Dr. Rennie and performed by the author with assistance from Dr. Rennie, Dr. Andrew Cornett, Alistair Rayner, Mitchel Provan, Nick Amlin, Rebecca Jacobs and Saber Ansari. The data and statistical analysis performed and presented in Chapter 2 was conducted by the author under the guidance of Dr. Rennie. Chapter 2 will be submit as a journal paper with the following authors: Brian Perry, Colin Rennie, Andrew Cornett, and Paul Knox. Chapter 3 was conceptualized by the author with assistance from Dr. Rennie and Dr. Cornett and the modelling completed by the author with guidance from Dr. Rennie and Dr. Cornett. Additional edits, comments, and reviews were conducted by Dr. Rennie and Dr. Cornett and led to the final iteration of this thesis.

2.0 Investigation of Large Woody Debris Impact on Structures and Debris Type Comparison in a Large Scale Physical Model

2.1 Introduction

Large wood (LW) has been a topic of research for nearly 50 years, with the goal of determining the impact that LW has on a river corridor. LW has the capacity to affect the channel geometry, flow rates, water level, sediment transport and the aquatic life that exists within this corridor (Wohl 2017). It is therefore no surprise that rivers with the potential for LW entrainment receive great attention concerning LW management. River managers attempt to assess the benefits that LW may provide a river ecosystem, and at the same time determine the hazards LW may pose to inhabitants and infrastructure of the surrounding area (Wohl et al. 2016). Of these hazards, flooding is of great concern. Flood damages can be aggravated by the presence of LW (Piton and Recking 2016). This creates a management challenge as LW recruitment and transport is a natural process that occurs within an environment yet directly increases the flood damage risks for this environment (Steeb et al. 2017). Examples of LW aggravating flood damages can be seen across the world, with the 2005 flooding in Switzerland (Steeb et al. 2017) but more recently with the 2013 flooding of Calgary, Alberta (Kappel et al. 2016).

Our current understanding of how LW becomes recruited into a river system and moves through the corridor can be conceptualized via the wood budget (Wohl 2017), which identifies areas where an extreme event such as flooding may increase the amount of wood being recruited or increase the amount of LW being transported from upstream into an area of concern. Once entrained, Large Woody Debris (LWD) has been shown to cause the most damage through debris accumulation at infrastructure such as bridges, weirs or culverts where debris can reduce or fully dam entire cross sections (Schmocker and Hager 2013). This accumulation increases water levels and can increase overall sediment deposition (Braudrick and Grant 2001), as well as local scour, further expanding the breadth of flood damages.

Following excessive rainfall in June 2013 (Pomeroy, Stewart, and Whitfield 2016), the City of Calgary, Alberta experienced significant flooding with damages exceeding $5 billion (Cornett et al. 2017)**.** These damages were exacerbated by LWD flowing within the river corridor. The Elbow River flows directly through the City of Calgary where it joins with the Bow River. The typical capacity of the Elbow River is 180$m^{3/}$s, but it conveyed flows up to 1240m^3/s during the flood event with an estimated return period

of 1:200 years (Cornett et al. 2017). LWD was observed within the river during floods but also a significant amount of LWD was observed along the riverbanks following the flood. The mean large diameter and length of the LWD from field investigations was equal to 0.44m and 16.5 m respectively (Cornett et al. 2017). Notable root wad was observed attached to the base of approximately 63% of debris.

The subsequent flood mitigation studies prompted a proposal to construct the Springbank Off-stream Storage Reservoir, whose purpose would be to store floodwater from the Elbow River temporarily and release it back into the system after flood recession. An overview of the proposed site location is available in Figure 1. In order to validate and improve the initial design of the Springbank project, the Ocean Coastal and River Engineering Research Centre at the National Research Council of Canada (NRC-OCRE) was commissioned to conduct a large-scale physical model study. The 1:16 scale physical model was used to assess and improve the initial design as well as investigate the behaviour of sediments and woody debris for a multitude of flow conditions. In order to investigate the damming of LWD at the structures, physical modelling experiments with scaled wooden debris were performed. Referencing previous works to help with selection of scaled debris types, it was evident that no industry standard exists. Designing scaled debris as smooth cylinders from wood (Rusyda 2015), or from PVC (Furlan et al. 2017) allows researchers to quickly create LWD for their models however lack the same roughness as natural wood, and in turn drag coefficients (Alonso et al. 2009) . Adding roughness elements, such as branches to these smooth cylinders (Davidson, MacKenzie, and Eaton 2015) or roots (Horiguchi et al. 2015) may increase their realism and yield different results when modelled. Using realistic debris has also been investigated (Schmocker and Hager 2011) yet these different scaled debris types are seldom investigated in tandem or their performances compared. Investigations have been performed in flume (Bocchiola, Rulli, and Rosso 2008) as well as in scaled rivers (Welber, Bertoldi, and Tubino 2013) and yet little consistency exists with modellers and their selected debris type. Therefore, this study investigates several debris types and if difference between these can be established it will enforce the idea that consideration should be given to the impact of debris type selection, both on previous and future studies.

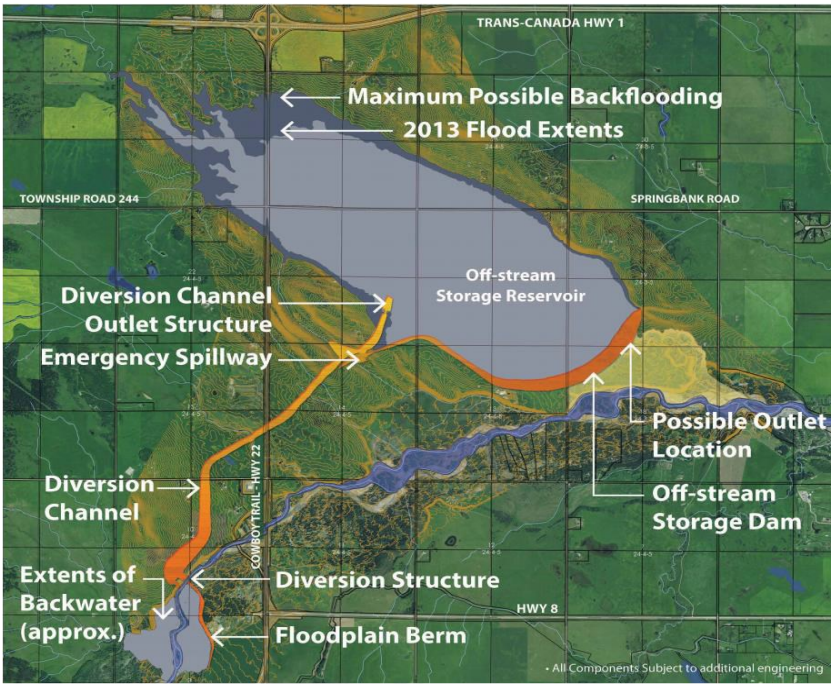

Figure 1: Overview of Springbank Project, outlining locations for flow structures and storage reservoir along the Elbow River upstream of the City of Calgary

2.2 Physical Model

The Springbank physical model was constructed within the Large Area Basin (LAB) at the NRC-OCRE facilities in Ottawa, Canada. The basin spans 50m by 30m and can accommodate water depths up to 1.4m. The basin is adjacent to a High Discharge Flume capable of generating flows up to 1.6m^3/s, and for this study the LAB was fitted with two adjustable weirs to control the downstream water level. A variety of instrumentation was utilized to monitor the performance of the model including water level gauges, Acoustic Doppler Velocimeters (ADVs), time-lapse photography and real time video recordings.

An undistorted length scale of 1:16 was implemented in the construction of the model as it minimized scale effects and maximized the extent of the model. Froude scaling was used to relate quantities within the model to quantities within nature as it was assumed that inertia and gravity forces dominated. A faithful scale model of the bathymetry and topography around the proposed project site was constructed within the LAB by erecting plywood templates in parallel lines at 1m intervals, backfilling with gravel and finishing the surface with grout. Forested areas were identified within the terrain and simulated by placing scaled tree limbs at a pre-determined density of 5 trees per 1m^2 within the grout. The model was designed and constructed to replicate future conditions at the site including the natural

river channel, a portion of the adjacent forested floodplains, a new dredged diversion channel and two new flow control structures.

2.2.1 Initial Design

The initial design consisted of a diversion inlet structure to regulate flow passing through the diversion channel and an adjacent service/spillway structure to regulate flow through the main (natural) channel. The structures were designed to accommodate various flow events up to the design peak flow of 1240 m^3/s. The main channel was designed to receive all flows up to 160 m^3/s and following exceedance of this flow rate, the diversion system would begin to divert waters from the main channel into the off-stream storage reservoir. Table 1 shows the design flows for the diversion and main channel as well as the flows used in the 1:16 scale physical model within brackets.

Table 1: Diversion and Main Channel Design and (model) Flowrates

Total Discharge (m^3/s)	Main Channel (m^3/s)	Diversion Channel (m^3/s)
160 (0.156)	160 (0.156)	0 (0)
320 (0.313)	160 (0.156)	160 (0.156)
760 (0.742)	160 (0.156)	600 (0.586)
1240 (1.211)	640 (0.625)	600 (0.586)

The initial design for the diversion inlet featured four 10m wide bays each separated by 2m wide piers with radial gates installed within each bay to control flow and chute blocks situated downstream to dissipate energy. The main channel structure consisted of a 10m wide sluiceway with radial gate for regulating flow during normal operating conditions and a 31m wide service spillway with Obermeyer Crest gates and a central pier. All dimensions were scaled by a factor of 16 for construction within the physical model. Riprap was placed directly in front of both structures and curved retaining walls were constructed on either side of the structures to match the initial design. Figure 2 displays a plan view of the initial design, flow direction and release locations for the debris testing.

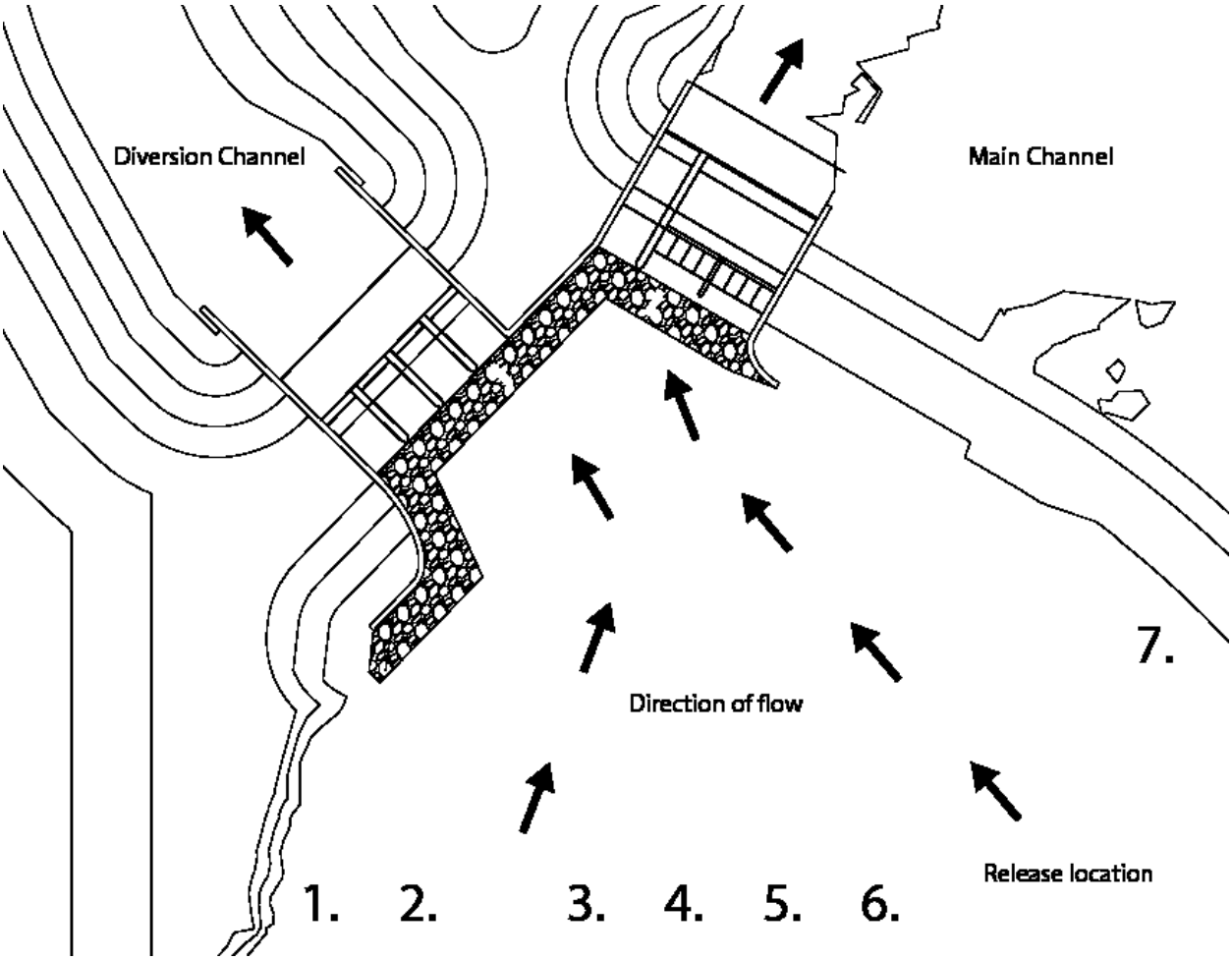

Figure 2: Plan view of the original structural design, with the diversion structure leading left and the main channel leading right. The seven release locations for debris testing are identified upstream of the structures.

2.2.2 Modified Design

A series of tests were conducted to calibrate flow conditions in the model and assess the performance of the initial structure designs in a range of flood scenarios, including the behavior of sediments and woody debris. Based on the outcome of these tests, it was decided to build and assess a very different alternative design in the physical model. The changes to the diversion inlet structure included decreasing the number of bays from four to two; resulting in two 20m wide bays with a single 4m wide central pier. The wider bays were necessary to minimize bridging of debris pieces between piers, which precipitated debris damming. The new pier nose was removable so that multiple nose designs could be tested, allowing the shape that could most successfully convey debris downstream to be identified. The radial gates were replaced with vertical lift gates.

The new flow control structure on the main (natural) river channel was also redesigned and relocated 30m upstream from its previous location. The new design featured two curved Obermeyer Crest gates w a central pier. The leftmost gate spanned 24m and the rightmost gate spanned 18m. The sluiceway present in the initial design was eliminated. Moreover, the curved retaining walls were optimized for improved conveyance of flow and debris. Figure 3 shows the realization of the second design in the physical model and highlights the modifications made to the initial design.

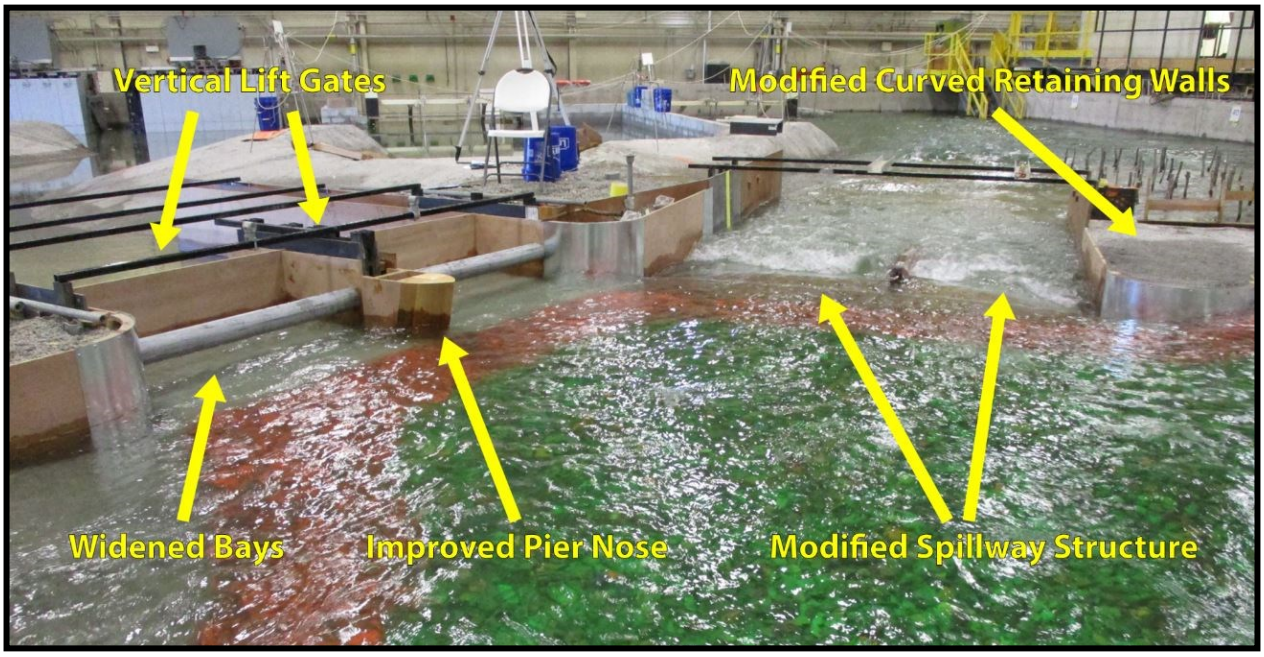

Figure 3: Modified Diversion and Spillway (Main Channel) Structure

2.2.3 Debris Barrier

A debris rack was designed and installed during some tests in order to investigate its ability to limit LWD entering the diversion system. The debris rack consisted of metal pipes firmly attached to a flat base. The spacing between each post was equal to 5m (full scale), with a total span of 38.2m. The rack was placed directly upstream of the diversion structure and anchored in place so that it remained stationary during damming events.

2.3 Large Woody Debris

The large woody debris used within the physical model was divided into three separate debris types:

- Manufactured Debris (MD) consisting of smooth cylindrical wooden dowels purchased from a manufacturer
- Realistic Debris with no Root Wad attached (RDN); real tree branches sorted and cut to length

- Realistic Debris with Root Wad attached (RDR); natural tree branches sorted and cut to length with the addition of a 10cm "X" shape made of two 3cm wide thin wooden strips stapled to the bottom to simulate a root wad. The root wad proved to be very durable through the course of testing and remained attached following multiple tests.

An example of the root wad attached to the debris as well as the debris during fabrication is available in Figure 4. The real debris had bark, kinks, knots and other abnormalities due to being cut and sized from tree branches. All debris pieces had similar lengths and diameters, as listed in Table 2.

Figure 4: Root Wad attached to LWD (left), debris fabrication at NRC facilities (right)

Table 2: Large Woody Debris Characteristics

Debris Type	Mean Length (m)	Mean Large Diameter (m)	Mean Small Diameter (m)	Mean Density (kg/m^3)
RDR	1.00	0.025	0.00875	652
RDN	1.00	0.025	0.00875	652
MD	1.00	0.025	0.025	399

2.4 Testing Method

Initial testing with debris was conducted to observe the interaction of LWD with the proposed flow control structures and quickly assess their performance during different flood conditions. The process for this assessment was to release the debris from an upstream location, as a mixture of both RDN and RDR pieces, and note the damming characteristics and interactions with structures. Release locations

varied based on the structure being investigated to optimize the number of pieces contacting the desired structure for each specific test. The number of debris pieces released also varied, with individual pieces and rafts of 2, 4, 10, 40 and 100 pieces being released. The debris pieces and their paths were tracked with time-lapse photography and videography. Following these tests (and others) the model flow control structures were modified as described above, and the more systematic test procedures described below were followed.

2.4.1 Debris Raft Testing

Debris rafts of various sizes were released from seven pre-determined locations upstream of the diversion and main channel. The rafts increased in size from 2 to 4 to 10 and finally 40 piece rafts were released for each debris type. The seven release locations were selected based on flow path mapping that had been previously completed in the physical model. The number of debris pieces passing the structure were recorded and removed prior to the release of the next raft. All debris pieces were released parallel to the flow path and no debris rack was in place. As the debris rafts had the potential to interact with forested floodplains, some debris did not arrive at the structure as they were caught upstream. For this reason, results for percent passing were determined using total debris passing the structure versus total debris arriving at the structure.

2.4.2 Repeatability Testing

A repeatability study was conducted for each debris type utilizing a single debris raft size and single release location. Specifically, ten piece rafts were released from location number 5 a total of 15 times for each debris type. Based on previous research on blocking probability, 15 tests per debris type was deemed suitable to represent the damming behaviour (Furlan et al. 2017). The debris rack was installed upstream of the diversion structure for all tests and the number of debris pieces passing the rack was recorded. Caught pieces were cleared prior to the next release. All debris pieces were released with the same orientation, parallel to the flow path.

2.4.3 Single Debris Testing

Single pieces of debris were released continually from release location 5 until 40 debris pieces arrived downstream where a debris rack was installed. The number of debris pieces passing the rack and their position within the release sequence was recorded. The debris was not removed from the rack until all 40 pieces arrived downstream. All debris pieces were released with the same orientation, parallel to the flow path.

2.4.4 Debris Jamming Classification

In order to investigate the impact of root wad, debris jamming was classified into three categories. Debris jamming was considered any instance where a piece of debris did not completely pass the diversion or main channel structures. The debris jamming categories are:

- Key Log: this jamming is defined as the instance where an initial piece of debris is lodged within the rack and proceeds to have debris accumulate on itself forming a dam. This only occurred when the debris rack was in place; meaning this jamming type was only applicable to the repeatability and single debris tests.
- Debris Roughness: This jamming is defined as any instance where a piece of debris fails to pass the structures due to its roughness and/or irregular shape (i.e., non-cylindricalness). This occurred when two pieces of debris entangled over the pier nose, when debris partially passed the key log dam but nonetheless was caught due to roughness, or any other instance.
- Root Wad: this jamming is defined as the instance where a debris piece fails to pass the structures due to its root wad. This may occur when the root wad was caught on a structure, or if the debris piece passed the key log dam but became caught solely on its root wad.

2.4.5 Time-lapse Photo Analysis

Following the physical model testing, an in-depth analysis of the time-lapse photographs was conducted using ArcGIS. The angles of departure and of approach for the single debris tests was determined and represented as a rotation angle (in clockwise degrees from vertical within the plan-view photo). The angle of approach was determined based on the position of the debris piece immediately before interacting with the dam or debris rack prior to a dam forming. The framerate for the cameras was equal to 0.5 Hz allowing for the angle of each debris piece to be known seconds prior to interacting with the dam. As the dams expanded upstream, so did the position at which the angle of approach was determined. Outlines of each dam from the raft and repeatability tests were drawn and the surface area of each individual dam was computed within ArcGIS for comparison amongst individual debris types.

2.5 Results

The debris raft testing allowed for the identification of the optimal release location for the repeatability and single debris tests. This location was release location 5 and was deemed the optimized location as following the 81 raft tests, debris from this location consistently arrived at the center pier of the diversion structure, resulting in the most debris/structure interactions. Debris jamming types for the

debris raft tests were determined by reviewing the time-lapse photographs available for all tests. Table 3 displays the debris jamming types for all tests. Total debris arriving at structure represents the sum of all debris pieces released for that test type that arrived/interacted with the structure.

Table 3: Debris Raft Test Jamming Results for Manufactured Debris (MD), Realistic Debris without Root Wad (RDN) and Realistic Debris with Root Wad (RDR)

Raft Size	Debris Type	Jamming Type		Total Debris arriving at Structure/Total released	% Debris Caught	% Debris Caught by Root Wad
		Roughness	Root Wad			
2	MD	0	0	14/14	0.00%	0.00%
2	RDN	0	0	14/14	0.00%	0.00%
2	RDR	0	2	14/14	14.29%	14.29%
4	MD	0	0	24/28	0.00%	0.00%
4	RDN	0	0	24/28	0.00%	0.00%
4	RDR	0	1	26/28	3.85%	3.85%
10	MD	0	0	70/70	0.00%	0.00%
10	RDN	0	0	55/70	0.00%	0.00%
10	RDR	1	2	50/70	6.00%	4.00%
40	MD	8	0	152/240	5.26%	0.00%
40	RDN	39	0	196/240	19.90%	0.00%
40	RDR	4	23	200/240	13.50%	11.50%

As seen in Table 3, in general, the larger the raft size, the greater probability of debris jamming. Debris roughness accounted for 100% of jams within the MD and RDN debris types as no root wad was present to cause jamming. Jamming due to root wad accounted for 100% of the jams within the 2 and 4 piece raft RDR test series, 66.7% of jams within the 10-piece raft test and 85.2% of jams within the 40-piece raft test. Figure 5 displays jamming due to both root wad and debris roughness during the raft testing.

Figure 5: 17 piece dam jammed due to root wad (left) 38 dam jammed due to debris roughness (right) with no debris rack in place

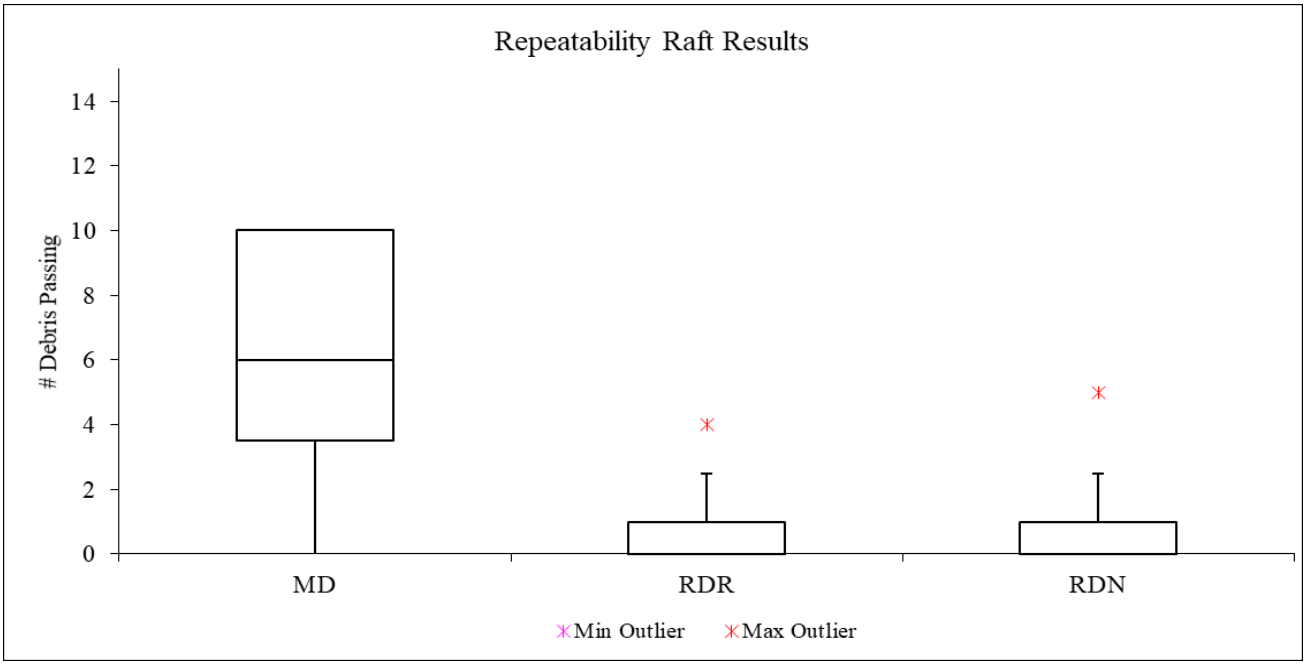

Figure 6: Repeatability Results: The largest/single box represents the median to the 75th percentile (Q3) of the data and the smaller box represents the 25th percentile (Q1) to the median (MD only). The whiskers are equal to 1.5 times the difference between Q3 and Q1.

From the Repeatability Raft tests, MD statistically significantly passed the debris rack more often than either RDN or RDR; based on students' T-test with 95% confidence (Figure 6). The mean number of pieces passing for MD was equal to 6.27 pieces per 10-piece raft while it was 0.87 and 0.67 for RDN and

RDR respectively. For the two realistic debris types, RDN saw a greater total number of pieces passing (13 vs 10) as well as a greater max outlier (5 vs 4).

Single debris results saw 20% of MD pass the debris rack, while only 5% of RDN and 2.5% of RDR passed the rack. The position within the release sequence for each debris type that passed the rack is available in Table 4. Only MD experienced debris passing the rack following the arrival of the 1st and 2nd debris piece at the rack. All debris types experienced a key log dam form following the arrival of the 3rd debris piece at the rack.

Table 4: Single Debris Test Results

	MD	RDN	RDR
LWD Released	40	40	40
LWD Passed	8	2	1
Sequence Position	1,2,13,15,26,27,28,29	1,2	1

Table 5 displays the angle at which the debris piece was released from location 5 within the single debris test and the angle at which it arrived downstream. These angles were determined through time-lapse photo analysis. Figure 7 represents the angle of arrival for MD (left) and RDR (right) in red, with all debris pieces exceeding one standard deviation from the mean drawn in yellow. As not all debris pieces were perfectly straight, the ends of the debris pieces were used to determine the angle of orientation.

Table 5: Angle of arrival and departure (from vertical) for single debris test (in degrees)

	RDR			RDN			MD		
	Mean	median	STDEV	mean	median	STDEV	mean	median	STDEV
Departure	-5.95	-3.52	13.82	-7.66	-9.01	15.03	-12.39	-12.43	13.23
Arrival	30.64	30.40	27.08	29.19	20.52	23.33	22.97	24.66	24.96

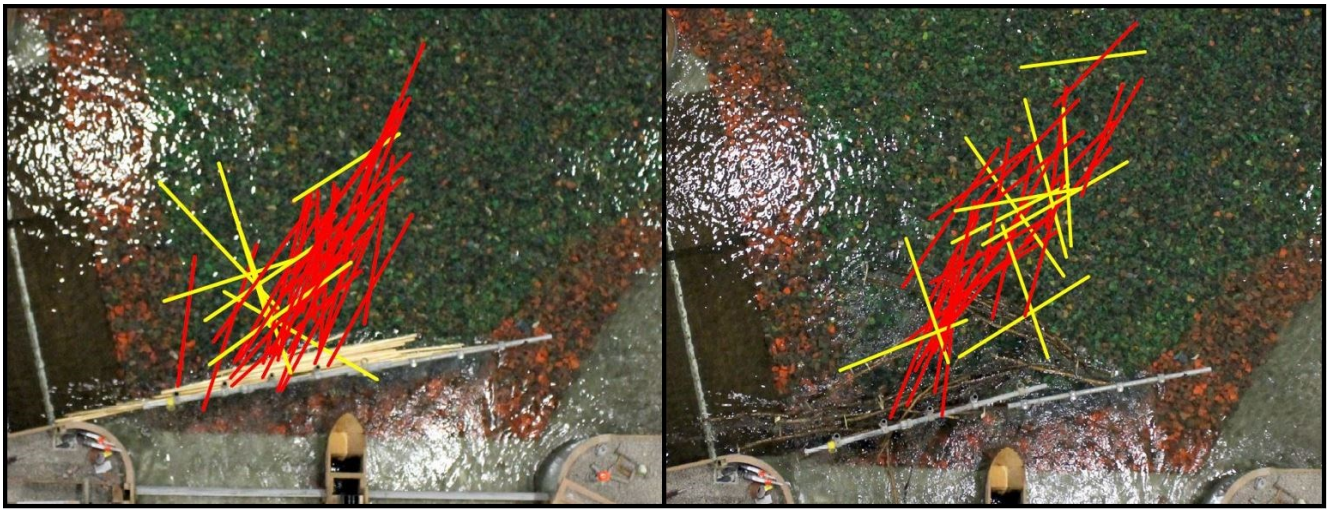

Figure 7: MD (left) and RDR (right) angle of arrival with pieces greater than one standard of deviation from the mean highlighted in yellow

Debris dam sizes varied for each debris test; however, on average RDR exhibited the greatest debris dam size. Dams were categorized by the number of debris pieces they contained and statistics were computed for all dams consisting of 9 debris pieces or more. For all 10 piece dams, 9 piece dams and also the single debris test, RDR had the largest average dam area and MD the smallest. Comparatively, in all but 2 of the 25 tests where dams consisted of at least 9 pieces, RDN or RDR exceeded the dam size of its MD counterpart. Figure 8 displays an outline of the dams formed for the single debris test as well as an outline of the dams formed for one of the 10 piece dam tests for each different debris type. Table 6 summarizes the dam area results.

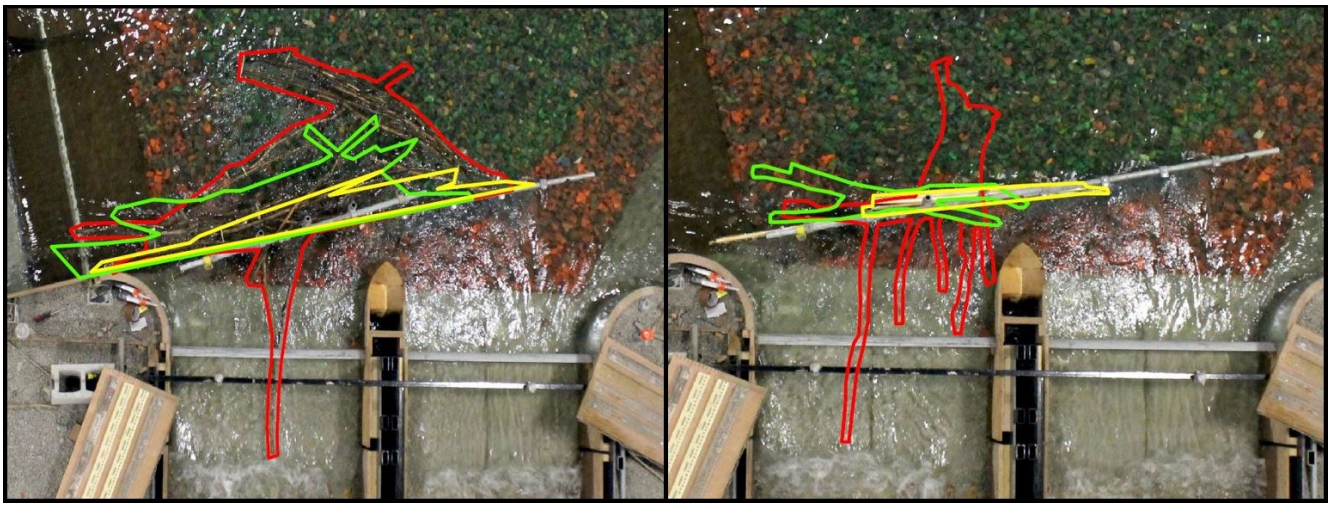

Figure 8: Outline of single debris test dam (left) and a 10-piece dam (right) for all debris types. MD yellow, RDN green and RDR red.

Table 6: 9 and 10 piece dam area statistics by debris type

Debris Type	Mean		Median		STDV		n	
	9's	10's	9's	10's	9's	10's	9's	10's
MD	0.191	0.099	0.191	0.099	N/A	N/A	1	1
RDN	0.245	0.245	0.246	0.221	0.046	0.062	3	8
RDR	0.253	0.269	0.243	0.269	0.08	0.06	6	8

The single debris test results (Table 7) did not have dams of equal debris pieces due to a greater number of MD passing the rack however the difference in debris dam area is significant when comparing RDR to MD and follows the trends observed within the repeated raft results.

Table 7: Single debris dam size and number of pieces

Debris Type	Area	# pieces
MD	0.324	32
RDN	0.740	38
RDR	1.495	39
Units	m^2	N/A

2.6 Discussion

2.6.1 Performance Assessment & Debris Structures

A large number of debris pieces interacted with the initial design structures and became dammed on the structure or caught in some other fashion. The most notable cause of this damming was the narrow bays of the diversion structure whose bays spanned a smaller length than the average length of the debris pieces. Debris pieces approaching perpendicular to the flow path were likely to become stuck at the entrance of the structure by spanning between two piers, creating a key log dam. Debris with root wad was also more likely to become stuck on the structures, especially those with sharp angles. Debris would approach parallel to the flow path and the roots would therefore approach perpendicularly, providing a point of contact to become stuck. The Obermeyer Crest gates exhibited this; however, it was dependent on water level. If the depth of water over the gates was less than the length of the root wad, it was observed that damming probability increased. The impact of blocking probability due to freeboard has been noted in other physical models investigating debris damming on bridges (Schmocker and Hager

2011); however, it was interesting to note the increased likelihood of blocking based on depth of water over gates.

The design modifications investigated in this study alleviated a large portion of the debris damming. The widening of the bays allowed perpendicular debris pieces to pass the structures, while the removal of the sluiceway and addition of the curved Obermeyer Crest gates removed sharp contact points for root wads to catch. Other modifications, such as moving the main channel structures upstream improved flow conveyance and in turn improved conveyance of debris through the structures. The debris rack, observed in the overhead photos, stopped 92.33% of realistic debris and 37.33% of manufactured debris from entering the diversion system. This was desirable as it was noted that debris stuck within the structure could impede normal operations of the gates.

2.6.2 Debris Type Comparison

Manufactured debris performed in a statistically significantly different manner than either of the realistic debris types. In every testing scenario, MD exhibited the least amount of debris jamming. The debris raft tests saw only 5.25% of debris that arrived at the structures jam, however some debris did not arrive at the structures due to jams upstream within the floodplain. Observing the repeatability results, MD had a mean number of pieces passing of 6.27, while both realistic debris had a mean less than 1. Single debris results were consistent with the other test results, with MD being the only debris to have more than 2 pieces pass the rack during the continual release. More importantly, it was the only debris type to have pieces pass following the formation of the dam, as the last piece to pass during the release sequence of 40 pieces was the 29th. The single debris test displayed the damming mechanisms of the different debris types well. As the pieces arrived at the rack, the first and second piece (for MD and RDN) passed the rack, however once the first piece jammed on the rack, the dam began to form. It proceeded to expand along the face of the rack and grow outwards. Realistic debris pieces would become immobilized within the dam upon contact; however, the MD pieces would contact the dam and continue to move along the dam face, flowing through the main channel structure. The shape of the dam for the realistic debris and manufactured debris also differed greatly. The number of perpendicular or angular pieces in the realistic debris dams far exceeded the number seen in MD.

2.6.3 Impact of Root Wad

Investigation of the impact of root wad on the performance of debris required meticulous review of the time-lapse photography in order to identify specific instances where debris jammed solely due to the presence of the wad. From the debris raft results, it is clear that root wad played a major role in the

debris jamming for this test. Of the 33 debris pieces that jammed for the RDR, 28 of them were caused by the root wad, accounting for 84.8% of the debris jamming. RDR was also the only debris type to jam during these tests in the smaller raft categories (2, 4 and 10 piece rafts). Other debris types also jammed during testing of larger rafts; however, the root wad still accounted for the majority of the jamming for RDR (23 of the 27 pieces caught during the 40 piece test). Identifying the impact of root wads within the repeatability test proved more difficult, as key log dams caused the majority of debris blockage when the debris rack was in place. However, the time-lapse photography showed that in 5 of the 15 tests for the RDR, 1 or 2 pieces of debris per raft would have passed the rack had root wad not been present. This accounts for an increase in blockage of 5.33% for RDR debris versus RDN.

2.6.4 Angle of Approach

Looking at the angle of approach for the single debris, it is evident that the angle varies greatly and that releasing debris pieces from a similar location/orientation upstream does not result in the same angle at the downstream end. This is likely due to the randomness of the turbulence within the model altering the rotation angle of individual pieces, while the mean flow path determines the location at which the debris pieces arrive. All debris collided with the debris rack; however, large variance could be seen in the angle of approach to the dam. The mean rotation angle was somewhat less for MD than for RDR or RDN (Table 7), but the standard deviations were too great to prove that the different debris types had statistically significantly different angles of approach. Interestingly, RDR had a somewhat greater standard deviation than RDN or MD. This increased variance does allow more debris to arrive at a greater range of angles and allows the dam to increase in surface area as the pieces arrive. Intuitively, if more debris pieces approach the dam at a greater span of angles the dam will likely be bigger in size, and this was the case.

Comparing these results to other physical models, some discrepancies exist. Most models with large woody debris note that the debris aligns itself quickly with the direction of the flow and that if root wad is present, the root aligns itself in the upstream position. This has been noted in both flume (Schmocker and Hager 2011) and non-flume based physical models (Welber, Bertoldi, and Tubino 2013). Based on the results of the angle of approach it is clear that the debris did not always align itself with the mean flow path. Again, it appears that turbulence within the model plays a greater role in determining the angle of approach to the structure.

2.6.5 Debris Dam Characteristics

Debris dams created from realistic debris greatly exceeded the surface area of its manufactured debris counterpart. Within the single debris test, the RDR debris had an area greater than four times that of the manufactured debris, while the RDN debris was more than twice that of the MD dam's surface area. In the repeatability tests for both 9 and 10 piece dams, RDR had the greatest mean dam surface area, followed closely by RDN. Both realistic debris types exceeded the mean dam surface area of the MD and based on the standard deviation of both realistic debris it is evident that realistic debris dams will consistently exceed those of its cylindrical counter parts by a significant amount. This increase in dam surface area can be attributed to the irregular shape of the debris pieces as well as the increased range of angles at which the debris arrived at the dam as discussed above. Previous research on debris damming has proposed estimates for dam volumes based on apparent surface area (Rusyda 2015). This research however utilized smooth cylindrical dowels in determining its empirical equation. Based on the results from this model, re-evaluating the empirical coefficients to adjust for debris that is more realistic may be required.

2.6.6 Scaling of Large Woody Debris

Scaling the LWD within the physical model was done with the intention to create model debris that was most similar to that observed in field however, some constraints still existed. Concerning the root wad attached to the natural debris pieces, this addition only simulated the volume of the observed root wad, increasing the debris piece angularity. In reality, this root wad has an increased density when compared to its stem, resulting in a weight distribution that would see the base of the debris being heavier than the tip. This was not observed in the physical model. The impact of density on blocking probability has been noted in other physical modelling studies of LWD (Furlan et al. 2017) and due to readily available materials, density differences existed between the natural debris and the manufactured debris. The manufactured debris proved to be lighter and less likely to become dammed. This result agrees with those from the (Furlan et al. 2017) experiment however this testing only considered one debris piece at a time and the difference in blocking probability was not as drastic as those observed within the Springbank model. It is likely that the density of the debris influenced the likelihood of damming and further investigations of the impact of density on damming of debris in rafts should be investigated. Nonetheless, the comparative nature of the experiments performed in the Springbank model demonstrate the extent to which the performance of realistic debris can differ from its cylindrical

counterpart. This leads the researchers to believe that the realistic debris with rood wad most accurately simulates the true nature of LWD.

2.7 Conclusion

The Springbank physical model study demonstrates that physical modelling is an excellent tool for design optimization and validation when the presence of large woody debris is a possibility. Numerous changes to the preliminary design to improve the conveyance of large woody debris were conceived, implemented, tested and confirmed in the physical model, and these refinements would likely not have been proposed or confirmed had no physical modelling been conducted. Once implemented, the conveyance of large wood pieces through both the main and diversion channels was greatly improved and minimal debris blockage occurred relative to the initially proposed design.

With respect to the performance of each debris type, it is clear that realistic debris made of natural tree limbs behaves in a different manner than manufactured cylindrical debris; a difference that is statistically significantly. The blocking probability of realistic debris far exceeded manufactured debris in all tests. The impact of root wad was also investigated and proved to be impactful, causing an increase in blocking probability when compared to the same realistic debris without root wad. Investigating the damming characteristics, realistic debris consistently created dams of greater surface area than manufactured debris. For these reasons, it is recommended that all large wood physical modelling be conducted with realistic debris comprised of natural tree limbs and that root wad be attached to an appropriate percentage of these debris pieces in order to ensure accurate results.

3.0 Numerical Model

3.1 Introduction

Following the completion of all physical model tests, a numerical model was created to investigate the flow characteristics of the Springbank project from a numerical perspective. As the project had an abundance of readily available data such as bathymetry and flow rates, ample information was available for comparison to numerical results to determine accuracy and aid in calibration. The principle objective for the numerical model was to investigate the accuracy to which it could simulate the physical model, with an emphasis being placed on the flow distribution between the main and diversion channel flow structures. From earlier physical modelling work, drogues (buoyantly neutral objects used to visualize flow paths) were released in the physical model and their paths tracked using time-lapse photography. Using ARC-GIS, these paths were then drawn and the dominant flow paths identified. Figure 9 displays an example drogue path from the physical model while the remaining drogue paths are available within the appendix.

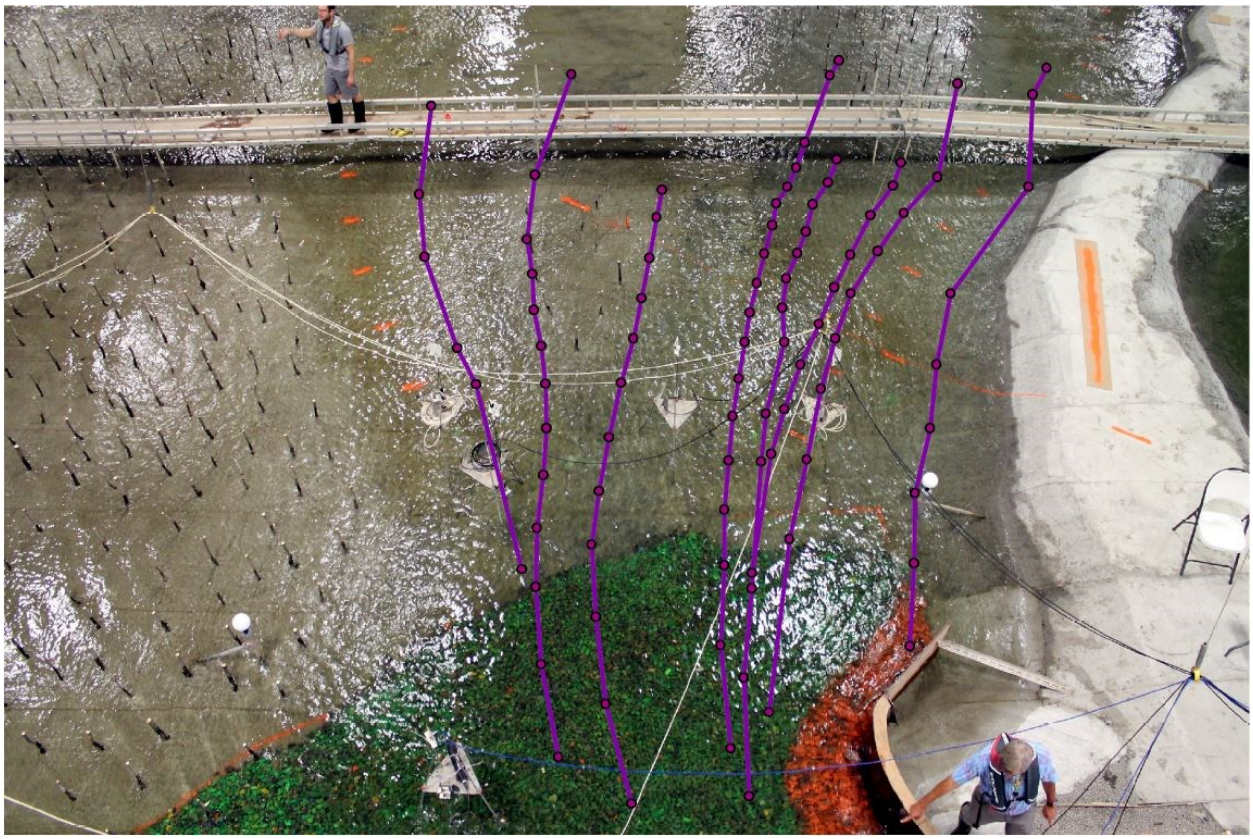

Figure 9: Drogue Paths for 760m^3/s flow condition

Using these drogue paths and the physical model data, it seemed attainable to develop a numerical model of the Springbank physical model and determine the degree to which a numerical system could simulate the flow distribution. It was recognized at the outset that numerical modelling of debris trajectories was beyond the scope of this Master's thesis research project.

3.1.1 Program Selection

The program selected for creating the numerical model was TELEMAC 2D from the open source suite of programs designed by TELEMAC-MASCARET. The two dimensional hydrodynamic program solves the Saint-Venant equation utilizing either finite element or finite volume methods to compute flow through each element of a triangular mesh (Leon and Gifford-Miears 2018). This program was deemed a suitable tool for simulating the flow distribution in the Springbank physical model due to its computational abilities as well as accessibility to the author.

Utilized in tandem with TELEMAC 2D was BlueKenue, a graphic user interface designed by the National Research Council of Canada that is capable of creating and modifying triangular meshes and displaying results from several open source modelling programs including TELEMAC 2D (Canadian Hydraulics Centre 2010). Combining these two programs, the author was able to generate and visualize results for the Springbank project.

3.2.1 Model Domain

Figure 10 provides an overhead view of the Springbank physical model. The model consisted of a high discharge flume where flow enters the model and two downstream weirs responsible for controlling water levels. The bathymetry data outline a main and secondary channel upstream of the flow structures, which then split into a diversion and main channel.

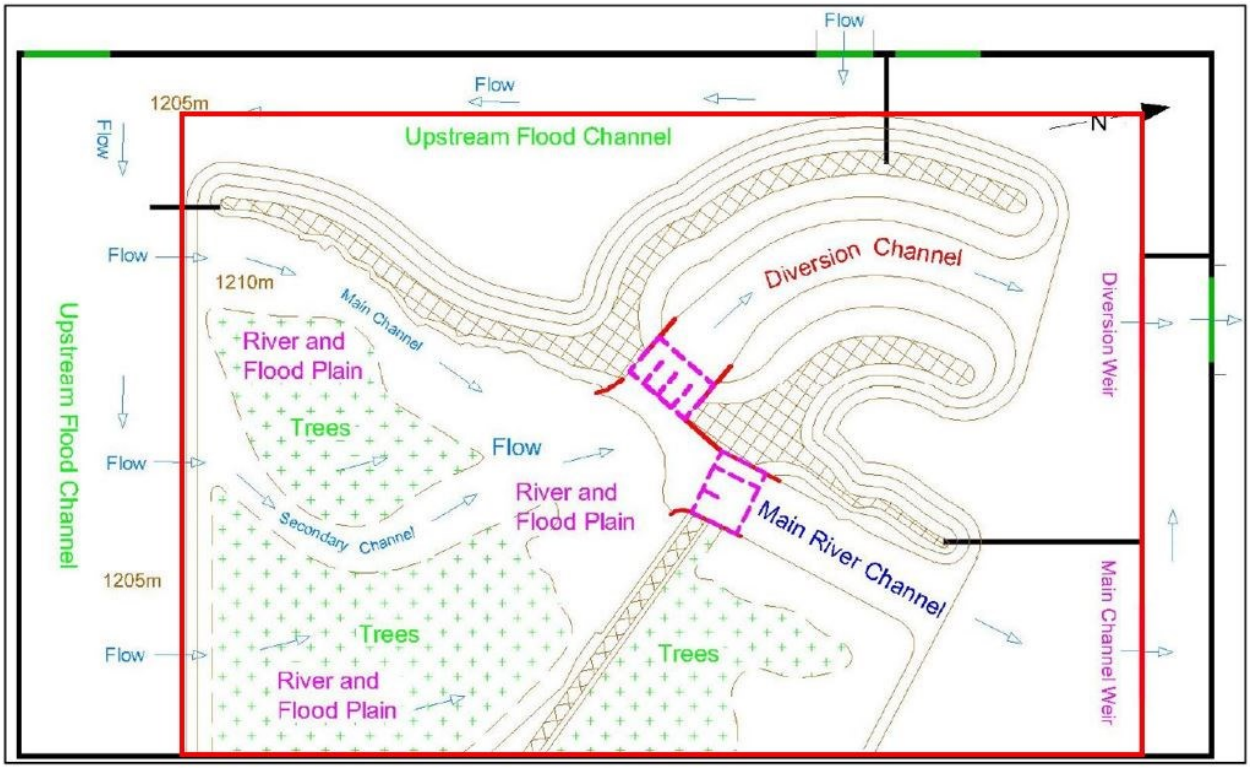

Figure 10: Springbank physical model layout with area to be modelled numerically outlined in red (NRC, 2016)

3.2.2 Model Data

Bathymetric data, which were used to create the templates for construction of the Springbank model, were available in the form of cross sections spanning the width of the large area basin at one-meter intervals. The bathymetric data were provided at model scale, meaning the total span of the data covered an area equal to 48m by 24.38m. Water gauges provided water level data for key locations throughout the model. The water levels at both the diversion and main channel weirs (Figure 11) were utilized to compute the flow (Figure 12) using the sharp crested weir equation; the summation of these flow rates was considered the total flow within the model. Velocity data were available for some locations of the model via Acoustic Doppler Velocimeters. Velocity time series at three sample locations are available in Figure 13 and are presented in prototype scale. Note the data acquisition system at NRC-OCRE provided the below figures and the author was not able to modify or edit the data or significant figures.

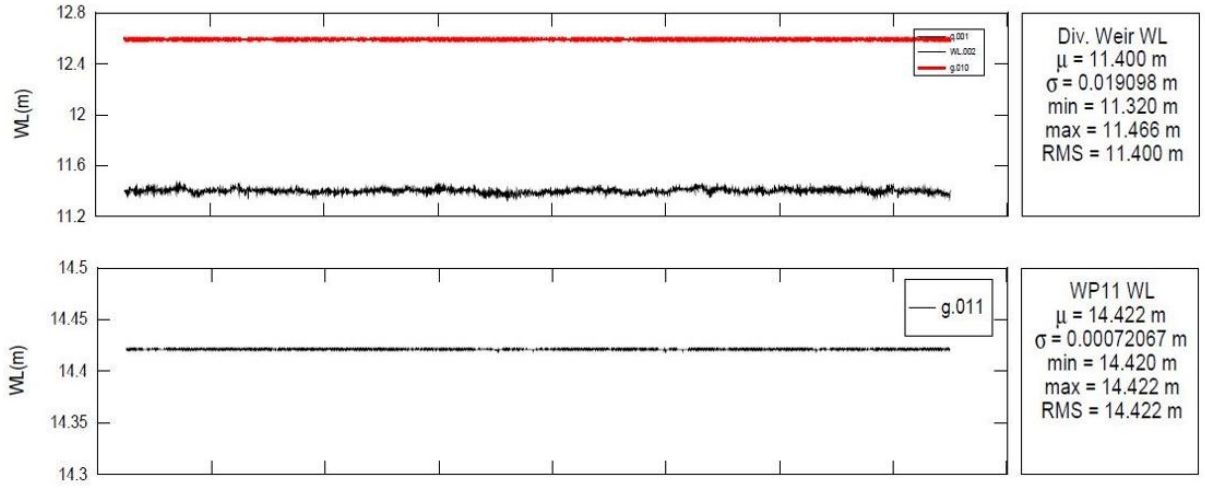

Figure 11: Water levels (m in prototype scale) for diversion and main channel (WP11) weirs from the physical model during the 760 m³/s scenario for 600s time interval

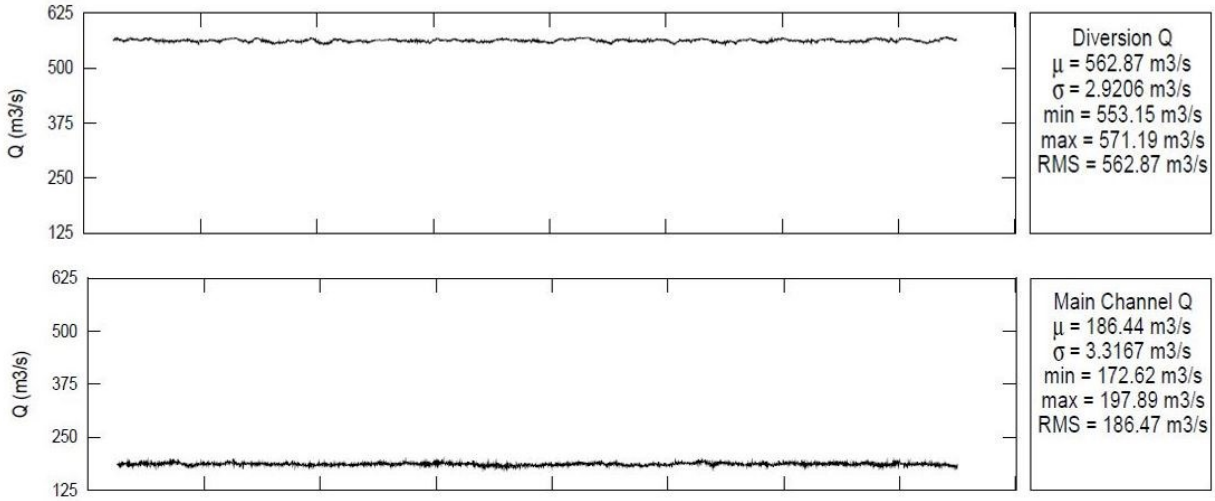

Figure 12: Flowrates (m³/s prototype scale) for diversion and main channel weirs from the physical model during the 760 m³/s scenario for 600s time interval

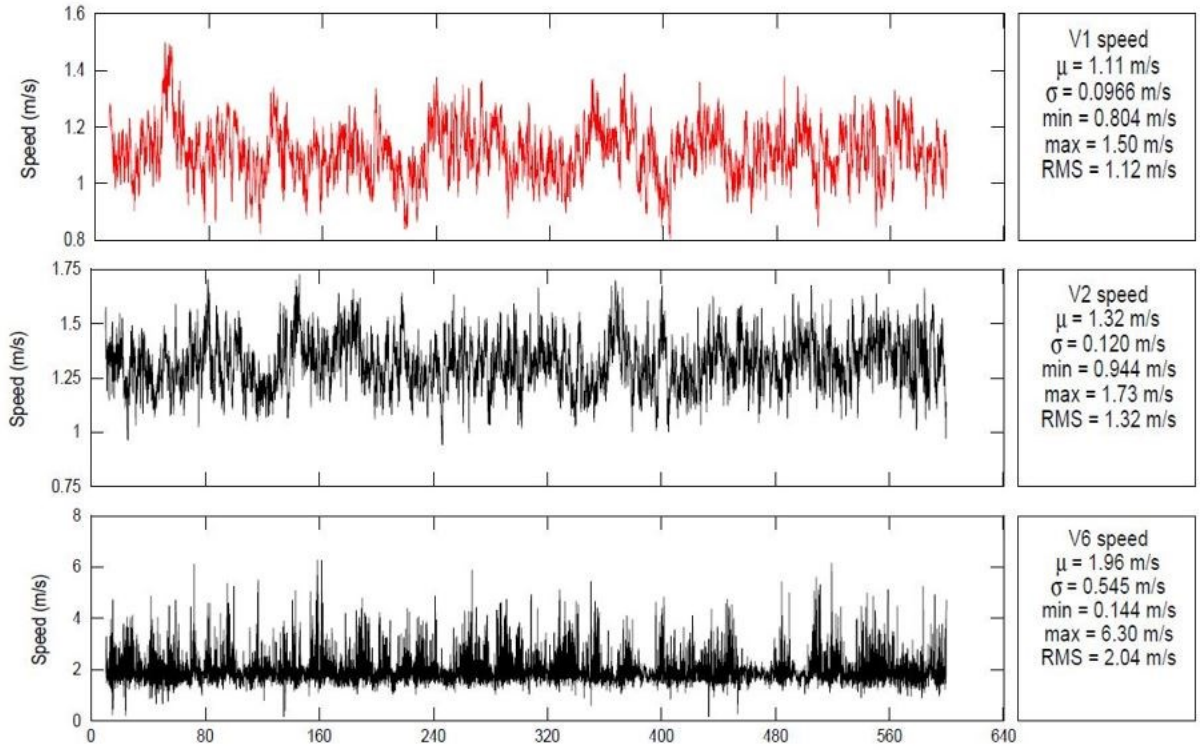

Figure 13: velocity data (m/s prototype scale) for ADV locations 1, 2, 6 from the physical model during the 760 m³/s scenario for 600s time interval

As the results were in prototype scale, the values being inputted into the numerical model required downscaling. Utilizing Froude scaling, the water levels, flowrates, and velocities were converted. Example conversions are available in Table 8 for prototype to model values. Recall the model scale (λ) is 1:16; no ADV filtering was conducted and mean values were used for all velocities, flows, and water levels.

Table 8: Example Froude scaling of quantities

	Prototype	Froude Ratio	Conversion	Model
Flowrate (m^3/s)	562.87	$\sqrt{\lambda}/\lambda^3$	$4/16^3$	0.549
Water Level (m)	11.4	$1/\lambda$	1/16	0.712
Velocity (m/s)	1.11	$\sqrt{\lambda}/\lambda$	4/16	0.278

3.3 Model Parameters

The model parameter values were selected to match the physical model, including flow rates and weir elevations. Several other model parameters, which were specific to the modelling program, were also required and are explained below.

3.3.1 Mesh Generation

Mesh generation was conducted using BlueKenue and utilized the bathymetric data provided from the NRC. Initial meshes consisted solely of the model domain however; the final, more defined mesh included an extended upstream reach to help flow develop prior to interacting with the model. Figure 14 displays a three dimensional view of the mesh used in generating results for the numerical model.

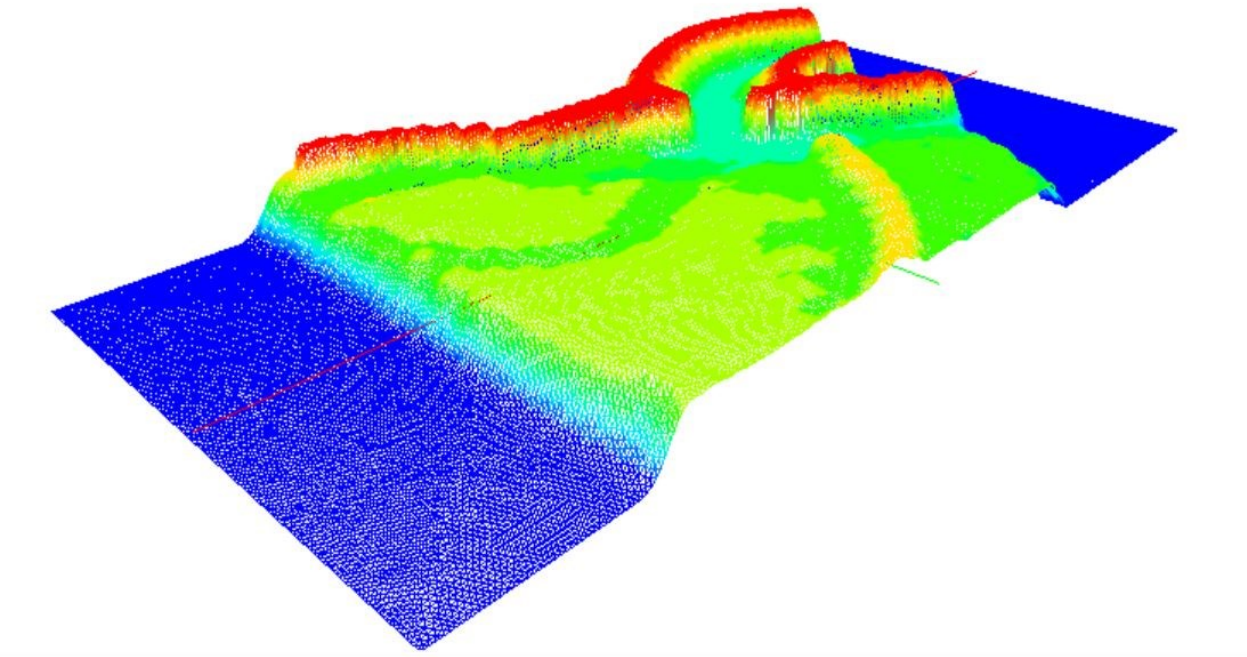

Figure 14: 3D view of the Springbank mesh used in numerical modelling

The final mesh used for the simulation allowed flow to develop 10 meters upstream prior to flowing over the incline (the incline was located directly upstream of the bathymetric data, where the deep blue transitions to green on both 3D and 2D meshes) and onto the bathymetry, similar to how the physical model was created. Table 9 displays the properties of the mesh including total element count and area statistics. The diversion flow structures were not incorporated into the mesh, as consideration of vertical

surfaces would have required drastically increased mesh resolution. This limitation is discussed further below.

Table 9: Element properties for the numerical mesh generated in BlueKenue

Node Count	Minimum Area (m^2)	Maximum Area (m^2)	Mean Area (m^2)
31494	0.007	0.035	0.0188

A mesh independence test was conducted by randomly selecting 100 points and sampling velocities for the above mesh and a more refined mesh with 57681 nodes. The points were compared for a selected time step after the model had fully converged and a total percent difference of 3.3% averaged over all points was achieved. The flowrates through the control sections and inlet were also compared and found to be within 2%. This was deemed an acceptable level of variance between the two and therefore the mesh used was sufficiently refined.

3.3.2 Boundary Conditions: Model Inputs, Outputs and Control Sections

The numerical model consisted of one input section, two output sections and two control sections. These can be seen in Figure 15. The input to the model simulated the approach conditions of the physical model and had a prescribed discharge. The input is located at the left end of the mesh in red. The outputs to the system, located at the right of the mesh in red, simulated the weirs of the physical model and had a prescribed elevation. The top output simulated the diversion channel weir and the bottom output simulated the main channel weir. The control sections of the model, in black, were used to determine the flow through the main and diversion channel. The locations of the control sections were selected as to capture all of the flow passing through the main channel and diversion channel downstream of where the structures were located. The diversion channel control section is the top black line while the lower black line represents the main channel control section. The purple dots represent the locations of the ADVs from the physical model, where velocity data were available. The probes are ordered as probe #1, #2 and #6 from left to right.

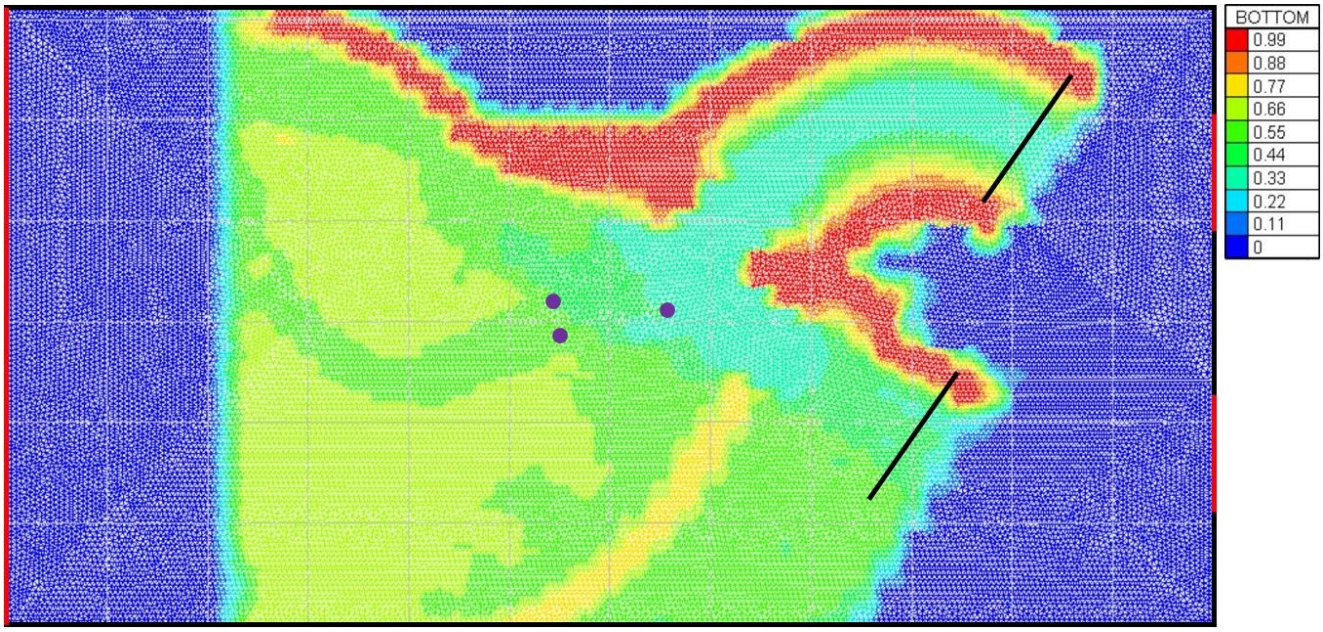

Figure 15: 2D view of numerical model mesh with control sections (black), input (left), outputs (right) in red and ADV locations (purple). The provided scale is in meters and represents the elevation of each node.

The values of the prescribed elevations and flowrates for the input and output sections are available in Table 10. As no prescribed flowrates were given to the output sections, they acted as free outfalls. The model was downstream controlled and therefore no water elevation was prescribed to the inlet. The selected downstream elevations were initially set to the scaled elevations from the physical model and then adjusted elevations were determined through calibration and resulted in the appropriate flow distribution through the main and diversion channel as seen in the physical model for the 760m^3/s flowrate scenario. These elevations represented the weir sill level. Only one flow condition was modelled (760m^3/s), which is the same flow condition at which all debris testing was conducted. Future works of numerically simulating debris would be conducted at this flow condition, thus this was the flow condition simulated.

Table 10: Prescribed Flowrates and Elevations for Numerical Model

	Elevation (m)	Flowrate (m^3/s)
Input	-	0.727
Diversion Channel Output	0.725	-
Main Channel Output	0.755	-

The remaining boundaries of the model (i.e. the walls) were considered closed boundaries where no flow could enter or leave the system. These boundaries as well as the model bottom had roughness coefficients assigned to them. A Chezy roughness coefficient of $50m^{1/2}/s$ was prescribed to the walls and a variable roughness was prescribed to the bottom of the model to simulate the forested regions of the model. Figure 16 displays the bottom roughness with the three forested regions represented in blue. After some calibration, a bottom roughness of $45m^{1/2}/s$ was selected for the majority of the model (red sections) and $17m^{1/2}/s$ for the forested regions (blue sections). This represents an approximate roughness ratio of 3:1 for concrete channels to floodplains with stumps (U.S. Department of Transportation 2013).

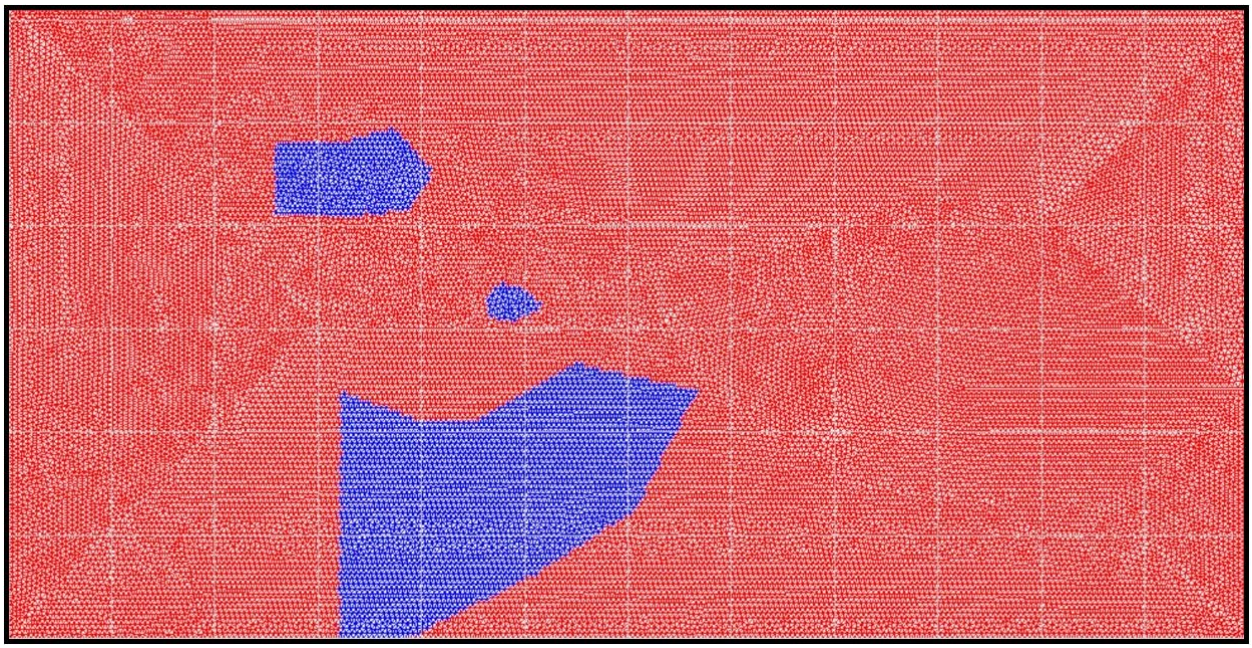

Figure 16: variable bottom roughness for numerical model with forested regions (blue)

3.3.3 Simulation Parameters

The run time for the numerical model was selected to equal 60 minutes, with 0.1-second time steps resulting in a total number of time steps of 36000. This time step was selected to maintain model stability as higher time steps resulted in exceedance of maximum iterations for computing flowrates and elevations. Outputs were graphically generated every twenty time steps resulting in a value available at every two seconds for the duration of the simulation. The turbulence model selected for the simulation was the K-Epsilon turbulence model available within TELEMAC 2D, which estimates a spatially varying eddy viscosity. This model assumes that the turbulence exceeds the dispersion occurring in the model; based on the physical modelling this was assumed to be true.

The simulation was hotstarted from a previous simulation with a simpler turbulence model. This was conducted to maintain model stability and decrease computation time. Flow rates remained constant between simulations and the K-Epsilon turbulence model was introduced along with drogue deployment at specified locations across the model.

3.3.4 Model Calibration

A two-step approach was taken for the calibration of the numerical model. Initially a simpler turbulence model (constant viscosity) was selected to ease computation requirements, and the downstream weir elevations were altered until the approximate flow distribution between the main and secondary channel was achieved. Once the flows were approximately equal to those seen in the physical model, the turbulence scheme was changed to the K-Epsilon model. Weir elevations were then adjusted to ensure the flow distribution was correct for the K-Epsilon model. Following calibration of the weirs, velocity readings were extracted at the three velocity probe locations and compared to those from the physical model. The roughness of the bed was then altered until the numerical simulation was within tolerance of the values seen in the physical model. The flow distribution was then checked to ensure it remained within tolerance and the weirs were adjusted if required.

3.4 Results

The numerical model yielded results for the entire simulation period of 60 minutes. As the simulation was a hotstart from a previous run, the first time step can be seen occurring at 2400s, due to the initial simulation having run time of 40 minutes. During the first 6 minutes of the simulation, the change in turbulence model and slight adjustments to the diversion channel water level causes variation in the flow rates. After approximately 6 minutes of run time, the flows begin to approach their steady state. Figure 17 displays the flowrates versus time for the diversion and main channel.

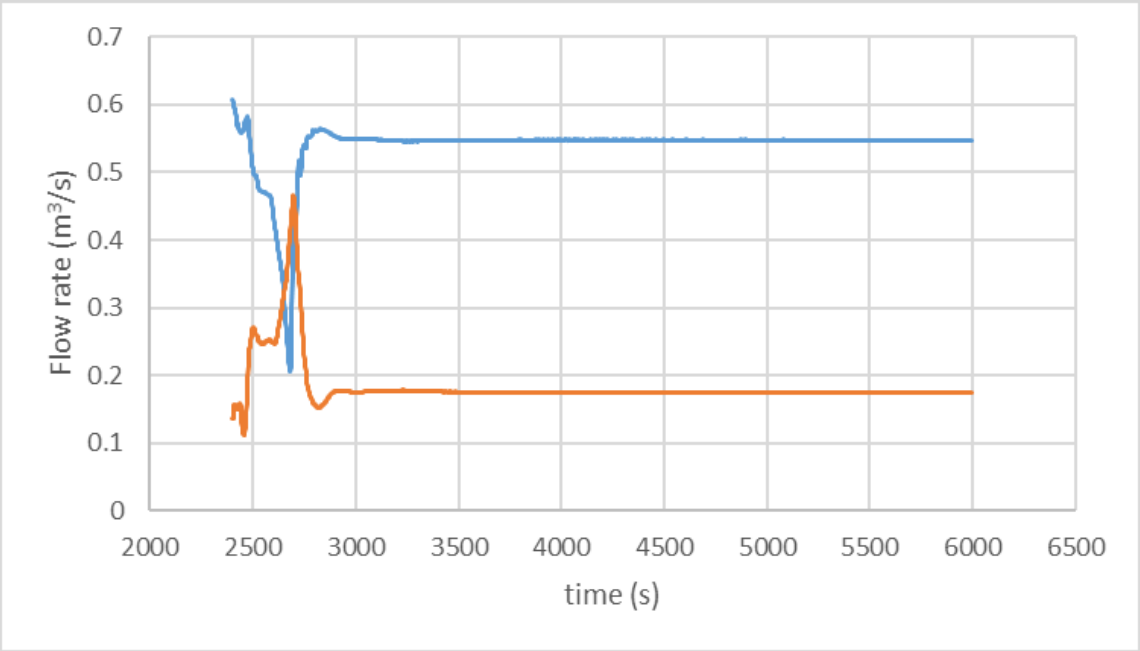

Figure 17: Flowrate through Diversion (Blue) and Main (Orange) channel control section

Table 11 summarizes the mean flow from the inlet, diversion and main channel for the time interval of 3000s to 6000s. The sum of the flow leaving the system (diversion plus main control) was equal to 0.723 m^3/s and is approximately 0.4% less than the flow computed entering the system. The values from the physical model are also provided in Table 11, and will be discussed further below.

Table 11: Summary of Diversion and Main Channel Flowrates

	Flow (m^3/s)	
	Model	Physical Model
Inlet	0.726	0.727
Diversion	0.548	0.542
Main	0.175	0.185

Figure 18 presents the velocity results at 0 and 60 minutes. The maximum velocity computed was equal to 0.819 m/s and can be seen in the upstream section of the model. Some secondary circulation can be seen in the downstream of the diversion channel as flow approaches the outlet and hits the wall of the large area basin. This was noted in the physical model.

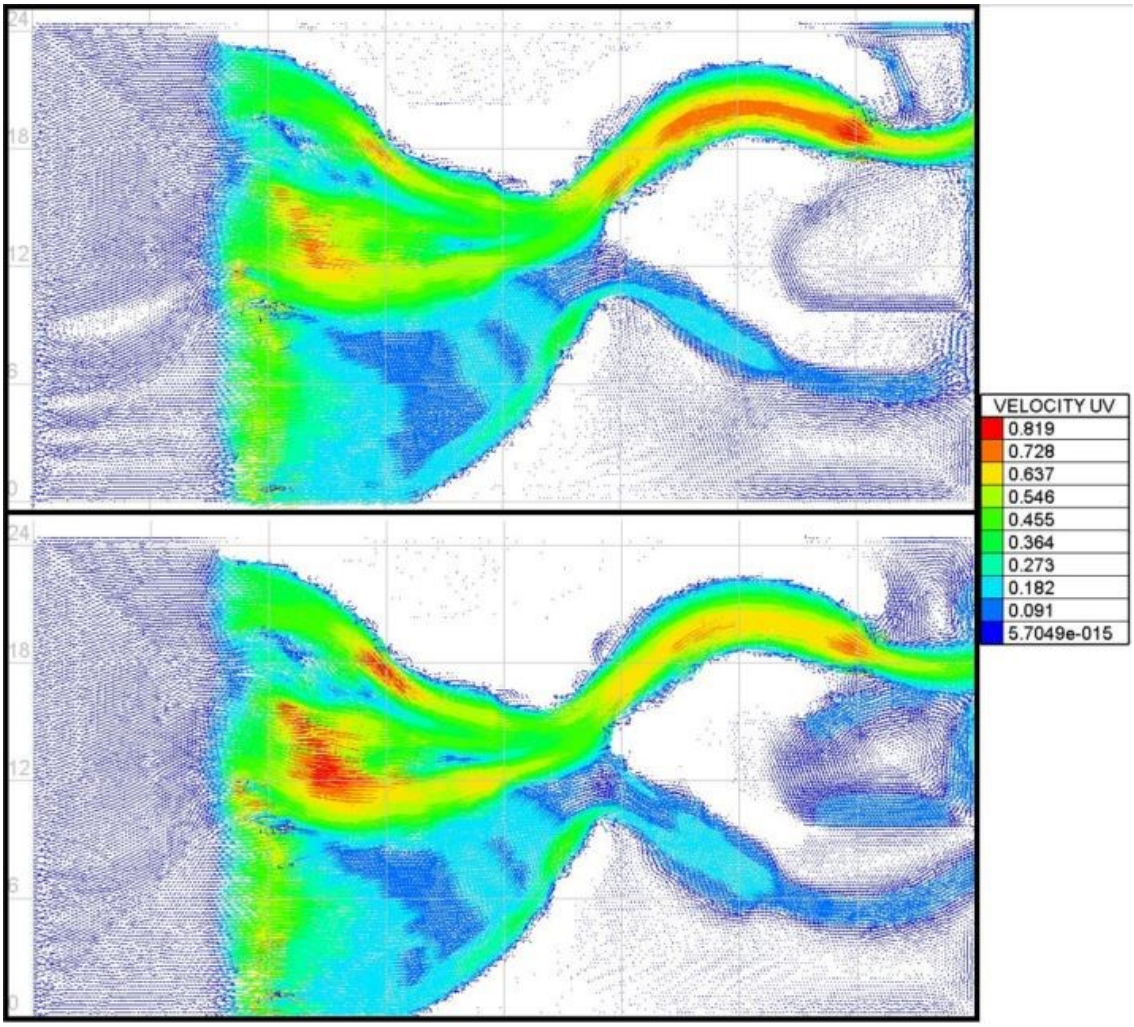

Figure 18: numerical simulation velocities in m/s at 0 (top) and 60 (bottom) minutes

Utilizing BlueKenue, the time series velocity data at each ADV probe location was extracted and the mean velocities computed. These velocities were used to calibrate the model to within a certain level of tolerance to values observed within the physical model. Table 12 presents the mean velocities from the numerical simulation and the physical model.

Table 12: mean velocity results for the physical (downscaled) and numerical model at probe locations 1, 2 & 6

Probe	Physical (m/s)	Numerical (m/s)
1	0.278	0.284
2	0.330	0.567
6	0.490	0.475

The pre-determined tolerance for the velocities was targeted at 5%. Following model calibration and slight adjustment of probe locations, both velocity probes #1 and #6 were brought to within 3% of its physical model counterpart. Velocity probe #2 however was not able to meet the tolerance level. This discrepancy is discussed further below.

Drogues were simulated in the model, their paths tracked, and then compared to the geo-rectified paths from the physical model. Seven drogues were released in the upstream of the model and their paths tracked until passing the flow diversion downstream. Figure 19 displays the drogues paths for both the numerical and physical model and helps to visualize the dominant flow path. The frequency of the position tracking was equal to 2 seconds for the physical model drogues (x's) and 0.5 seconds for the numerical model drogues (squares). Each point represents a time-step in the overall path taken by a drogue. Figures 20 and 21 show an enhanced view of the main/secondary upstream channel and the floodplain respectively. The scalar flowrates for the numerical simulation at 60 minutes is also available and presented in Figure 22.

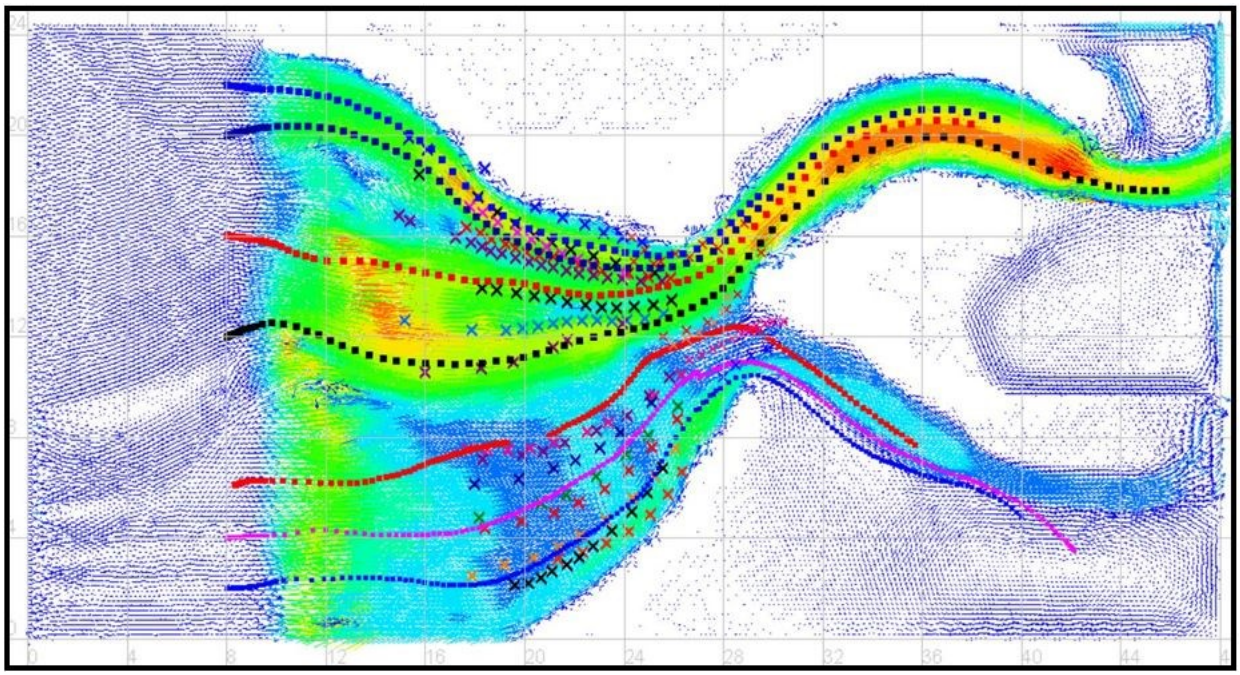

Figure 19: simulated drogue paths overlaid onto velocity results at 60 minute time step. Numerical drogues represented as squares and physical drogues represented as X's. The velocity colour scale is the same as in Figure 18.

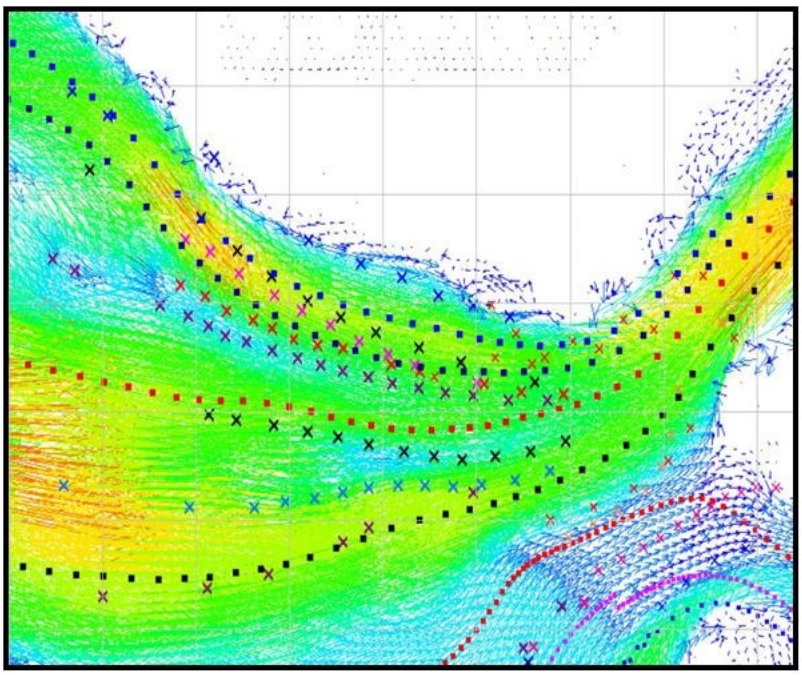

Figure 20: Drogue paths for main and secondary upstream channel. Squares (Numerical) and X's (Physical) represent the drogue at each time step. The velocity colour scale is the same as figure 18.

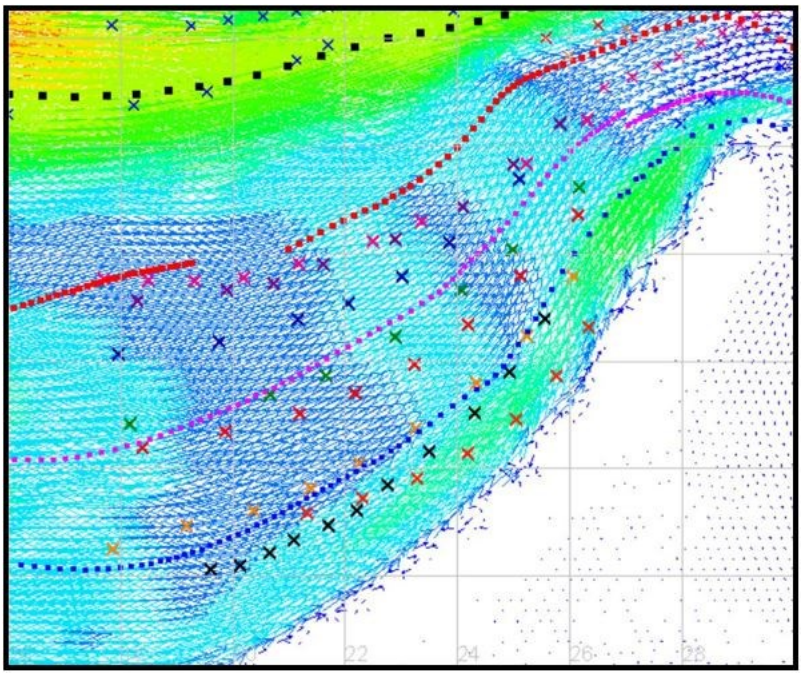

Figure 21: Drogue paths for floodplain. Squares (Numerical) and X's (Physical) represent the drogue at each time step. The velocity colour scale is the same as figure 18.

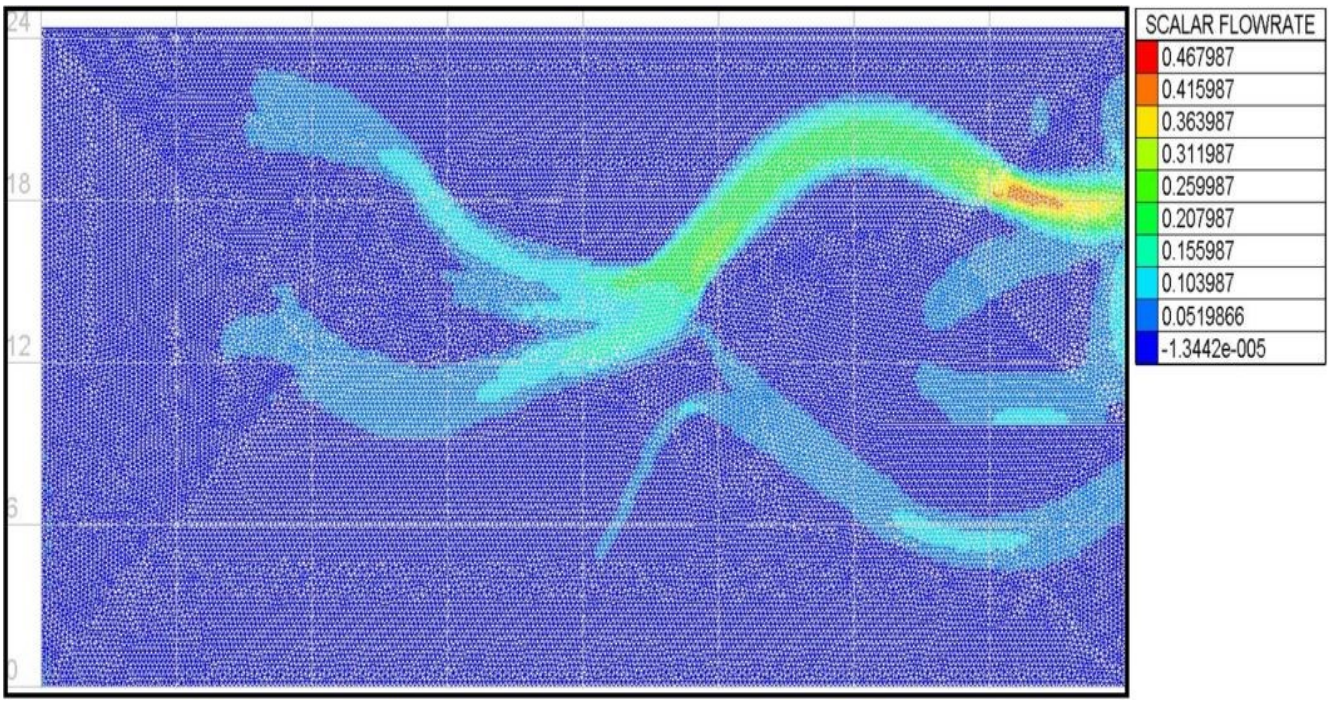

Figure 22: Scalar flowrate at 60 minute time step (m^2/s)

The largest flow computed in the simulation was equal to 0.476 m^2/s and can be seen in the diversion channel as the flow proceeds down the slope onto the LAB floor. The scalar flowrates help to visualize the dominant flow paths where the majority of the flow proceeds downstream.

3.5 Discussion

The flow distribution and velocities simulated in the numerical model closely reflect those seen in the physical model. By adjusting downstream weir elevations, the average flow through the diversion channel was calibrated to be within 0.3%, and within 1.5% for the main channel, of the physical model values. The average total flow entering the system was within 0.03% of the physical model values. The simulated flows were thus very reasonable in terms of error. In order to obtain these values, however, the simulated weir sill elevations did not match exactly the weir sill elevations used in the physical model. The main difference in weir sill elevations was in the main channel where the numerical elevation was 0.755m as compared to a physical model elevation of up to 0.9m. These elevation changes, which were determined through calibration of the model, were necessary, because no flow diversion structures were simulated. These structures regulated water levels at their location in the physical model; without them it was necessary to alter the numerical weir elevations to ensure proper flow distribution between the main and diversion channels. Implementing the flow structures within the

numerical model would allow for downstream water elevations more similar to the physical model; however, integrating them into the mesh proved to be a challenge. Data for the structures existed in the form of structural drawings but was not readily available in a similar data format as required for mesh integration. More importantly, extreme mesh refinement would be required around the flow structures in order to simulate the numerous right angles in their design, greatly increasing computation time for the model. Perhaps an improved approach would be the creation of a second model with a smaller domain, focusing solely on the flow structures. This nested model could then use the results from the current larger model to determine its boundary conditions. However, the majority of the model and the focal point for flow path mapping exists upstream of the flow structures, so their inclusion within the mesh was not crucial and the results obtained are still relevant.

Assessing the velocity results for the three probe locations, two of the three probes achieved very similar results to the physical model. Probes #1 and #6 were calibrated to be within 3% of their physical model counterparts. Probe #2, however, showed much higher velocities in the numerical simulation and could not be calibrated to within tolerance using local roughness coefficients. This led to an investigation on the validity of probe #2's location in the physical model, and if the recorded velocity results were reasonable. Reviewing the physical model drogue path mapping for the same flow condition (Figure 9), it appeared that the flow through the secondary upstream channel was significantly higher than through the main upstream channel. Probe #1's (main channel) and probe #2's (secondary channel) velocities were then confirmed via the mapped drogue paths. Based on Figure 9, the meter interval spacing drawn onto the model bathymetry (orange markers), and the sampling frequency of the flicker cameras (0.5 Hz), a ratio between the two probes could be established. From the physical model drogue paths, the approximate velocity ratio was 1:1.64 for probe #1 to #2. The physical model velocity data from the ADVs yields a ratio of 1:1.19, which is significantly lower. Using probe #1's velocity, which was equal in both numerical and physical models, and applying the ratio from the physical model drogue paths, the actual velocity at the position of probe #2 would be approximately 0.46m/s, not 0.33m/s. This value of 0.46m/s still sits below the numerical result 0.567m/s; however, the percent difference sits just above the 5% tolerance at 5.21%. This leads the author to believe that the flows within the secondary channel were higher than the ADV suggests, as confirmed by the drogue paths mapped physically and the numerical results. Potential reasons for the lowered ADV velocity include change in orientation, with the ADV probe not being aligned upstream as well as a drift in the calibration over the course of testing.

Additional velocity discrepancies between the numerical and physical models could arise because the numerical simulation is a two dimensional model, and thus yields depth-averaged velocities. The physical model results, on the other hand, depend upon the elevation of the ADV probe in the flow. Placing the ADVs at 40% depth above the bed, where the mean velocity for the profile would occur if the profile follows the log law of the wall, may minimize some errors. Still, discrepancies are expected. A 5% tolerance is reasonable when accounting for these differences.

The numerical drogue paths followed similar trends to those exhibited by the drogue paths mapped in the physical model. This is to be expected, as the velocities throughout the model were similar. It was interesting to compare the results of a truly neutrally buoyant drogue (numerical) versus that of a relatively buoyancy neutral drogue (physical model) as it was observed in very low flow that the drogue within the physical model would saltate along the bathymetry of the physical model and not remain suspended as in higher flows. However, once the physical and numerical drogues were overlaid, it was apparent that the drogues followed very similar paths upstream of the structures in both the main channels and floodplains. All drogues within the floodplain travelled at lower rates than those seen in the main channel and had a similar curve to that of the berm installed downstream and forced water to flow into the diversion structure. The physical model drogues approached closer to the berm than the numerical however, this was due to a design change made following the physical model drogue tracking which saw the berm move three feet upstream. Therefore, these drogues were allowed to move further downstream than their numerical counterpart. Assessing the main and secondary channel, we can see that again the two drogue types behave very similarly. Some flow paths have overlapping drogues from the two models further enforcing the idea that the numerical simulation was accurately able to model what was seen in the physical. Unfortunately, in order to compare velocities additional processing would be required as the flicker rate (rate at which photos were taken in the physical model) may fluctuate around the defined 0.5Hz, causing inaccuracies for the values of the physical model velocities.

Figure 23 shows the physical model drogue paths at the flow structures for seven drogues that were released upstream in similar locations to those in the numerical model. The same split of three drogues into the main channel and four into the diversion channel occurs in both models. The rate at which the drogues are moving is faster through the diversion channel than the main channel, and can be determined based on the distance between each point. This is true for the numerical model as well. Interestingly, two drogues within the physical model crossed paths as they approached the diversion channel, and this was not observed in the numerical model. It is difficult to draw quantitative

comparisons for the flow path mapping as the physical model results had flow structures in place and the numerical did not, but it is reassuring to see that regardless of flow structures, similar drogue splits are occurring in both models.

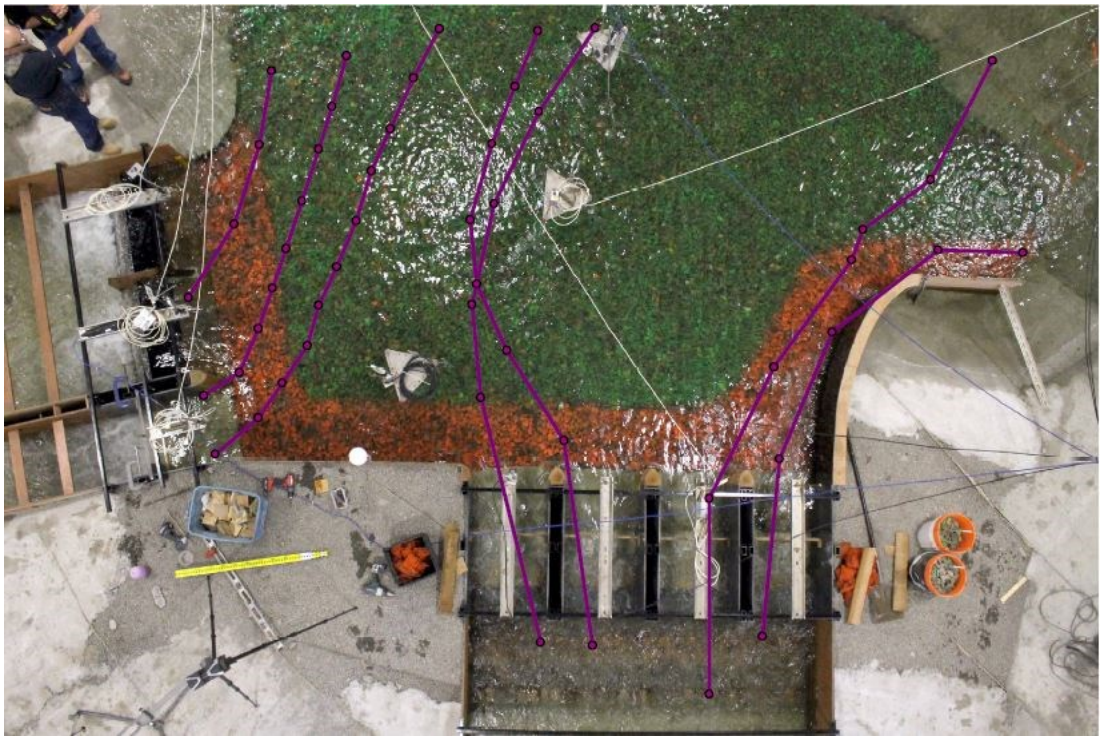

Figure 23: Drogue paths at confluence from physical model at 760m^3/s flow condition

TELEMAC 2D is a widely used and heavily validated modelling program, and as such was assumed to be flow conservative (i.e. flow entering the model equals flow leaving). During calibration and mesh independence tests this was confirmed through the use of control sections placed directly upstream of the main and diversion outlets, and directly downstream of the inlet. The slight difference of 0.4% between the inflow and the sum of the main and diversion controls outflow for the calibrated model can be accounted for through the computation error of TELEMAC 2D, which provides a warning that slight variations exists. *"The weak formulation of the no-flux boundary condition through solid boundaries raises a theoretical problem for computing the flow rates. Either they are compatible with the results file, or they are compatible with the weak formulation. To be compatible with the weak formulation, use the key-word COMPATIBLE COMPUTATION OF FLUXES. The difference may reach a few percents."* (Lang 2010). Therefore, in order to utilize control sections and receive compatible results files, a degree of inaccuracy and therefore some additional tolerance is required.

The varied roughness in the model allowed for calibration of localized velocities to a high degree of accuracy where velocity data were available. Roughness coefficients were used for the riverbed and for forested regions in the model; however other areas of varied roughness do exist and could be implemented into future models. The LAB floor was considerably smoother than the bathymetry fabricated from concrete, which was smoother than the riprap placed in front of the flow structures. If more velocity data were available for these locations, more coefficients could be introduced and calibrated to provide increased accuracy to the model.

3.5.1 Model Limitations

The numerical model provided an initial look at what was studied physically. However, some limitations did exist in the numerical model due to several factors including availability of data, program constraints, and so on. The flow diversion structures constructed in the physical model were not simulated due to issues of implementation into the mesh. These structures controlled flow through both the diversion and main channel and definitely affected the flow distribution between the two channels. These structures altered the water levels in the model and it was therefore required to calibrate the numerical simulation with different weir sill elevations than utilized in the physical model. Additionally, riprap was present upstream of these structures and an increased local friction coefficient would be required to represent this riprap. This was not modelled, as the velocity data for this section was inaccurate due to the lack of flow structures, and will be considered in future works.

The upstream portions of each model differed. The numerical upstream was designed in an effort to have a uniform distribution of flow into the model whereas the physical model was constrained by the facilities in which it was constructed, forcing a significant 90-degree turn directly before entering the model. This was not replicated numerically, nor were the flow straighteners used by the physical model. No data were available for the approach conditions in the physical model to act as a guide for the numerical model.

3.6 Conclusion

A numerical model was created in TELEMAC 2D which was able to simulate the same flow distributions seen in the physical model. Flow was accurately distributed using the bathymetry and downstream water levels within 0.3% difference for the diversion, which carried the majority of the flow, and 2% difference for the main channel conveying significantly less flow. The velocities within the simulation were similar in magnitude and location to those seen in the physical model; barring one of the sampling locations, velocity errors sat well within tolerance of less than 3% difference. This was achieved by

implementing varied bottom roughness coefficients throughout the model to simulate the forested areas of the model. Flow paths for the model were mapped using drogues that were released upstream of the model and their placement tracked as it progressed downstream. These were then compared to the geo-rectified drogue paths from the physical model and were determined to have similar trends. In order to conduct velocity comparisons, additional analysis of the flicker photography is required and will be considered for future work. No flow diversion structures were simulated in the numerical model and future models should incorporate these into the system. Nonetheless, this model acts as an excellent initial reconstruction of the Springbank model and shows the ability for TELEMAC 2D to simulate complex free surface flows.

4.0 Thesis Conclusions

The physical modelling work conducted in this thesis was intensive and of very large scale relative to much of the other work conducted in this discipline. The author was fortunate enough to be involved in such a project and it provided a unique opportunity to perform a novel investigation of the impact of large woody debris on flow structures and the importance of debris selection in physical modelling. A comparative analysis was conducted of three debris types that had not previously been conducted. The results of this analysis showed that modelling large woody debris with smooth cylindrical dowels was not representative of what is seen in nature. Creating debris for physical modelling using material harvested from natural trees proved more realistic and the results were found to be statistically significantly different. Additionally, it was determined that the inclusion of root wad on the natural debris proved to affect its performance in the model. Debris with root wad attached to its base was less likely to pass debris structures, had a greater variance in the angle of approach to the debris structures, and formed larger dams once jammed on debris structures compared to its root-less counterpart. The percentage of debris with root wad attached to its base was determined by post flood field investigations to be over 60%, thus it is important to consider root wads when physical modelling.

Based on the results from this work the author recommends that any physical modelling of large woody debris be conducted with debris fabricated from natural resources, or be engineered to be of equal roughness and have equally irregular shape. Field investigations should be performed to determine the dimensions of the debris as well as the percentage of debris that has root wad attached and this information should translate directly to the scaled physical model debris being tested. From the Springbank model, several major design changes were made due to the impact of large woody debris on the flow structures, which would have not been identified in clear water tests or numerical modelling. Results from previous physical modelling work on large woody debris conducted with smooth cylinders should be used with reservation as it has been proven that a large discrepancy exists between the performance of these cylinders and natural debris. If no root wad was considered in the modelling process, it may be advisable to include additional factors of safety to account for the performance differences in rooted and un-rooted debris.

The numerical modelling work conducted provided an excellent foundation for model refinement and comparison of numerical to physical results. The flow distribution of the numerical model through the main and diversion channel represented that seen in the physical model, while other key areas such as the confluence and upstream main/secondary channels were apparent. Localized roughness was introduced into the model and allowed for the calibration of velocities for two of the three velocity probes to be within 3% of its physical model counterpart, while the third probe suggested having some deficiencies with its data and if corrected showed velocities similar in magnitude to the numerical model. Drogue paths were simulated in the numerical model and they displayed similar trends to those from the physical model. Continued calibration following the addition of the flow diversion structures would likely result in a high quality model with the potential for debris simulation in the future.

5.0 Recommendations for Future Work

Due to the contractual nature in which OCRE-NRC operates, the Springbank model was only available to the author for a limited amount of time to perform tests and acquire data. The testing procedures created were therefore designed to optimize the time presented to the author but were not comprehensive. Furthermore, following data analysis and reflection on the strengths and weaknesses of this thesis, it became apparent that some improvements could be made and that future works are to be recommended. For the physical modelling, it was noted that in the field the density of root wad is greater than that of the stem of the debris. This results in a weight distribution that differs from what was modelled in the Springbank project and it would be interesting to the see the impact that having a heavier root wad would have had on the percent passing, debris dam formation, and angle of approach. Similarly, the investigation of the impact of density on blockage probability was investigated by (Furlan et al. 2017) for a single debris piece and it would be have been interesting to see the impact that density has on debris in rafts. This leads directly into an improvement to the physical model testing. The densities of the smooth cylinders and natural debris were not equal. This was due to readily available resources, and in hindsight having more density similar debris types would have eliminated a characteristic in which the debris types differed. This was not seen as a main contributor to why the debris types behaved in a statistically significantly different manner. Nonetheless, it is still an area in which the study could improve.

Echoing the points made in the conclusion for the numerical model, the addition of the diversion flow structures and calibration of velocities with localized friction coefficients in this vicinity will increase the accuracy of the numerical model. Future works for numerical simulations should aim themselves towards creating a nested numerical model with flow structures. Concerning the drogue paths, analysis of the flicker rates and determining the physical model drogue velocities should be conducted for use in a quantitative comparison of numerical to physical drogue velocities. An additional and perhaps more ambitious future work includes the introduction of a debris piece into the model to study its flow path. As numerous single debris tests were conducted and tracked using time-lapse photography, these can be used as a basis in which to compare the accuracy of the debris once simulated. To ease the matter, the debris being simulated would not have a complex shape as the smooth cylindrical dowel can be modelled based on known exact cylindrical dimensions. This is currently not possible within TELEMAC 2D; however, demand for this feature is high and in discussion within the river engineering research community.

6.0 References

Abbe, Timothy B and David R Montgomery. 1996. “Large Woody Debris Jams, Channel Hydraulics and Habitat Formation in Large Rivers.” *Regulated Rivers Research & Management* 12 (23): 201–21. https://doi.org/10.1002/(SICI)1099-1646(199603)12:2/3<201::AID-RRR390>3.0.CO;2-A.

Abt, Steven R., Syndi J. Dudley, and J. C. Fischenich. 1998. “Woody Debris Influence on Flow Resistance.” *Wetlands*.

Alonso, C V, F D Shields Jr, and D M Temple. 2009. “Dynamics of Large Wood: A Prototype Scale Flume Experiment.” *33rd IAHR Congress: Water Engineering for a Sustainable Environment*, no. October: 5151–58.

Alonso, Carlos V., F. Douglas Shields, and Darrel M. Temple. 2005. “Experimental Study of Drag and Lift Forces on Prototype Scale Models of Large Wood.” *Impacts of Global Climate Change, Proceedings of World Water and Environmental Resources Congress 2005*, 1–11. https://doi.org/10.1061/40792(173)581.

Bocchiola, D., M. C. Rulli, and R. Rosso. 2008. “A Flume Experiment on the Formation of Wood Jams in Rivers.” *Water Resources Research* 44 (2): 1–17. https://doi.org/10.1029/2006WR005846.

Braudrick, Christian A., and Gordon E. Grant. 2001. “Transport and Deposition of Large Woody Debris in Streams: A Flume Experiment.” *Geomorphology* 41 (4): 263–83. https://doi.org/10.1016/S0169-555X(01)00058-7.

Canadian Hydraulics Centre, NRC. 2010. “Blue Kenue.” *National Research Council of Canada*, no. August.

Cornett, Andrew, Paul Knox, John Menninger, Rick Lux, and Mitchel Provan. 2017. “Assessment of Debris Issues Impacting Design of a Flood Diversion Project in a Large Scale Physical Model” 6865 (1): 2232–40.

Davidson, S. L., L. G. MacKenzie, and B. C. Eaton. 2015. “Large Wood Transport and Jam Formation in a Series of Flume Experiments.” *Water Resources Research*. https://doi.org/10.1002/2015WR017446.

Ettema, Robert, Marian Muste, A. Jacob Odgaard, and Ozan Abaci. 2007. “Outflow Calibration for Vertically Distorted Models of Thermally Stratified Reservoirs Etalonnage Du Soutirage Sur Modèle Verticalement Distordu de Réservoirs Thermiquement Stratifiés” 44 (4): 535–47.

Furlan, Paloma, Michael Pfister, Jorge Matos, and Anton J Schleiss. 2017. “Blocking Probability of Driftwood at Ogee Crest Spillways with Piers: Influence of Woody Debris Characteristics.” *Proceedings of the 37th IAHR World Congress August 13 – 18, 2017, Kuala Lumpur, Malaysia.* 6865 (2016): 2357–64.

Gallisdorfer, Michael S., Sean J. Bennett, Joseph F. Atkinson, S. Mohammad Ghaneeizad, Andrew P. Brooks, Andrew Simon, and Eddy J. Langendoen. 2014. “Physical-Scale Model Designs for Engineered Log Jams in Rivers.” *Journal of Hydro-Environment Research* 8 (2): 115–28. https://doi.org/10.1016/j.jher.2013.10.002.

Hafs, Andrew W, Lee R Harrison, Ryan M Utz, and Thomas Dunne. 2014. “Quantifying the Role of Woody Debris in Providing Bioenergetically Favorable Habitat for Juvenile Salmon.” *Ecological Modelling* 285: 30–38. https://doi.org/10.1016/j.ecolmodel.2014.04.015.

Horiguchi, T., H. Shibuya, S. Katsuki, N. Ishikawa, and T. Mizuyama. 2015. “A Basic Study on Protective Steel Structures against Woody Debris Hazards.” *International Journal of Protective Structures* 6 (2): 191–215.

Kappel, Bill, Syed Abbas, Sal Figliuzzi, Seifu Guangul, John Menninger, and George Sabol. 2016. “ASSOCIATION CANADIENNE DES BARRAGES UPDATING PMP FOR THE ELBOW RIVER : COMPLEX TERRAIN , UNIQUE.”

Knox, Paul, Andrew Cornett, and Mitchel Provan. 2016. “Physical Model Study of the Springbank Off-Stream Storage Project Diversion Structure on the Elbow River.”

Kramer, M., W. L. Peirson, R. French, and G. P. Smith. 2015. “A Physical Model Study of Culvert Blockage by Large Urban Debris.” *Australian Journal of Water Resources* 19 (2): 127–33. https://doi.org/10.1080/13241583.2015.1116184.

Lang, P. 2010. “TELEMAC-2D Software Release 7.0 USER MANUAL,” no. October: 1–6.

Largiader, A Zischg A. 2011. “Modelling Woody Material Transport and Deposition in Alpine Rivers,” 425–49. https://doi.org/10.1007/s11069-009-9492-y.

Leon, Arturo S., and Christopher Gifford-Miears. 2018. “Evaluation of the PG Method for Modeling Unsteady Flows in Complex Bathymetries.” *Journal of Applied Water Engineering and Research* 6 (2): 139–49. https://doi.org/10.1080/23249676.2017.1287017.

Mazzorana, B, L Marchi, M Cavalli, B Gems, T Gschnitzer, and L Mao. 2018. “Assessing and Mitigating Large Wood-Related Hazards in Mountain Streams : Recent Approaches” 11: 207–22. https://doi.org/10.1111/jfr3.12316.

Pagliara, Stefano, and Iacopo Carnacina. 2010. “Temporal Scour Evolution at Bridge Piers: Effect of Wood Debris Roughness and Porosity.” *Journal of Hydraulic Research* 48 (1 EXTRA ISSUE): 3–13. https://doi.org/10.1080/00221680903568592.

Piton, Guillaume, and Alain Recking. 2016. “Design of Sediment Traps with Open Check Dams. II: Woody Debris.” *Journal of Hydraulic Engineering* 142 (2): 04015046. https://doi.org/10.1061/(ASCE)HY.1943-7900.0001049.

Pomeroy, John W., Ronald E. Stewart, and Paul H. Whitfield. 2016. “The 2013 Flood Event in the South Saskatchewan and Elk River Basins: Causes, Assessment and Damages.” *Canadian Water Resources Journal* 41 (1–2): 105–17. https://doi.org/10.1080/07011784.2015.1089190.

Ravazzolo, Diego, Luca Mao, Bruno Mazzorana, and Virginia Ruiz-villanueva. 2017. “Brief Communication : The Curious Case of the Large Wood-Laden Flow Event in the Pocuro Stream (Chile),” no. February: 2053–58.

Rusyda, Muhammad Islamy. 2015. “Log Jams at a Bridge with a Pier and a Bridge without Pier.” *Procedia Engineering* 125: 277–83. https://doi.org/10.1016/j.proeng.2015.11.040.

Schmocker, Lukas, and Willi H. Hager. 2011. “Probability of Drift Blockage at Bridge Decks.” *Journal of Hydraulic Engineering* 137 (4): 470–79. https://doi.org/10.1061/(ASCE)HY.1943-7900.0000319.

Schmocker, Lukas, and Willi H. Hager. 2013. “Scale Modeling of Wooden Debris Accumulation at a Debris Rack.” *Journal of Hydraulic Engineering* 139 (8): 827–36. https://doi.org/10.1061/(ASCE)HY.1943-7900.0000714.

Steeb, Nicolas, Dieter Rickenmann, Alexandre Badoux, Christian Rickli, and Peter Waldner. 2017. “Large Wood Recruitment Processes and Transported Volumes in Swiss Mountain Streams during the Extreme Flood of August 2005.” *Geomorphology* 279: 112–27. https://doi.org/10.1016/j.geomorph.2016.10.011.

U.S. Department of Transportation. 2013. “HEC-22, 3rd Edition Urban Drainage Design Manual.” Vol. 2009.

Villanueva, Virginia Ruiz, Geoscientific Prospective, and Geological Engineering. 2014. “Two-Dimensional Modelling of Large Wood Transport during Flash Floods” 449 (August 2013): 438–49. https://doi.org/10.1002/esp.3456.

Ward E.Sanford, Gerolamo Casile, Karl B.Haase. 2015. “Water Resources Research.” *Water Resources Research* 51: 9127–40. https://doi.org/10.1002/2014WR016259.

Welber, Matilde, Walter Bertoldi, and Marco Tubino. 2013. “Wood Dispersal in Braided Streams: Results from Physical Modeling.” *Water Resources Research* 49 (11): 7388–7400. https://doi.org/10.1002/2013WR014046.

Wohl, Ellen. 2017. “Bridging the Gaps: An Overview of Wood across Time and Space in Diverse Rivers.” *Geomorphology* 279: 3–26. https://doi.org/10.1016/j.geomorph.2016.04.014.

Wohl, Ellen, Brian P. Bledsoe, Kurt D. Fausch, Natalie Kramer, Kevin R. Bestgen, and Michael N. Gooseff. 2016. “Management of Large Wood in Streams: An Overview and Proposed Framework for Hazard Evaluation.” *Journal of the American Water Resources Association* 52 (2): 315–35. https://doi.org/10.1111/1752-1688.12388.

Appendix A: Debris Orientation Angles and Dam Outlines

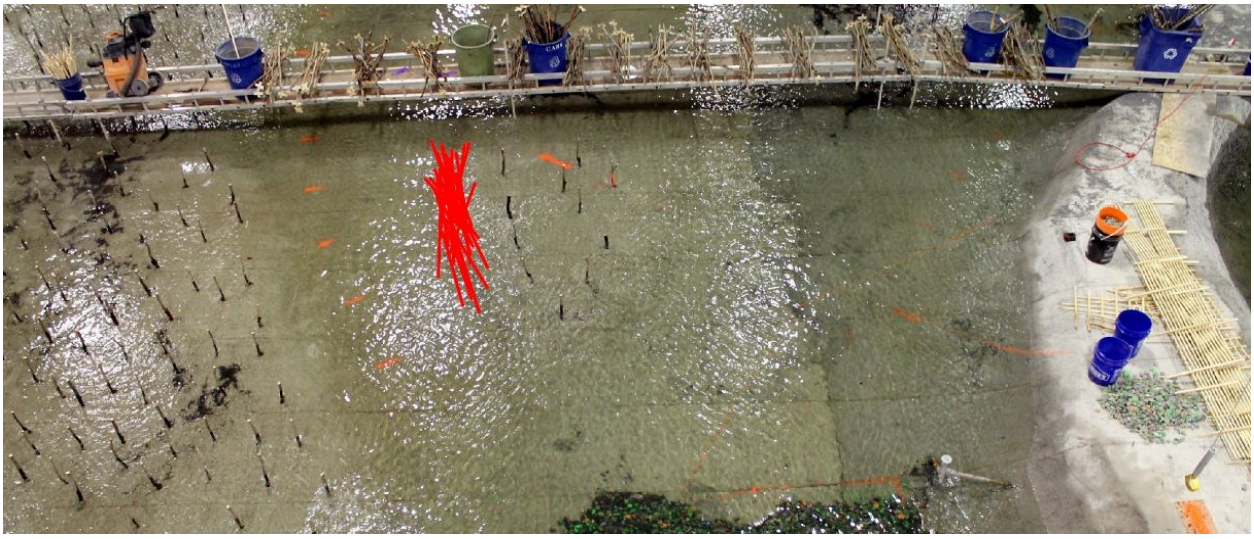

Figure 24: Angle of Departure for MD

Figure 25: Angle of Departure for RDN

Figure 26: Angle of Departure for RDR

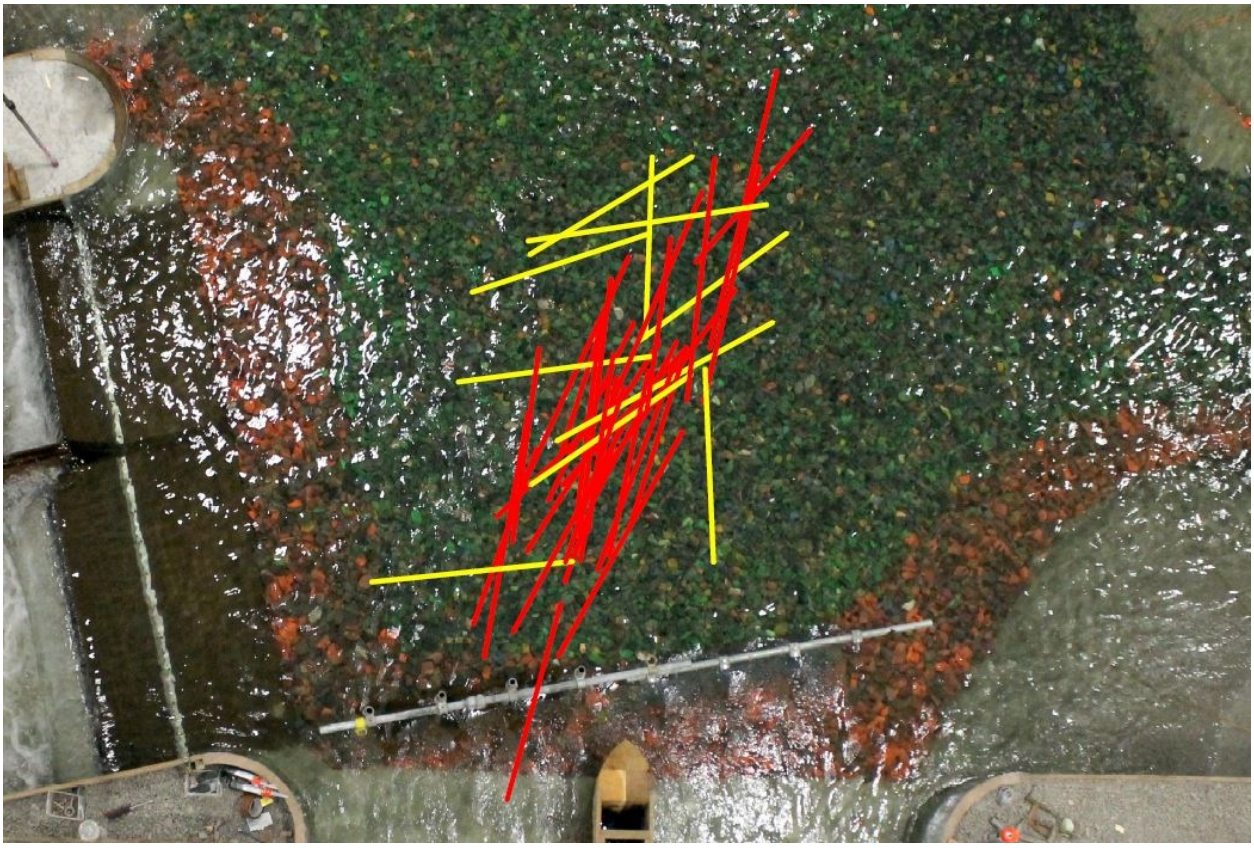

Figure 27: Angle of Arrival for RDN, Debris outside of one standard deviation of the mean highlighted in yellow

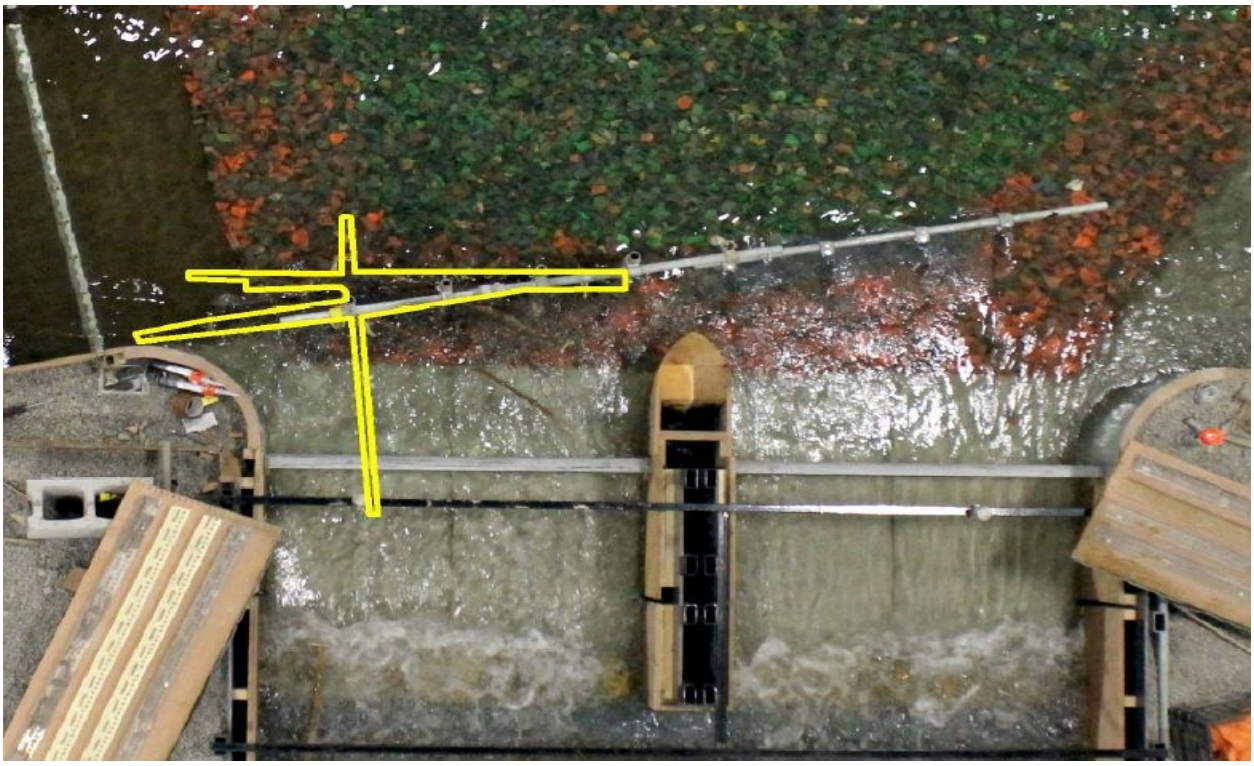

Figure 28: 9 piece dam for MD

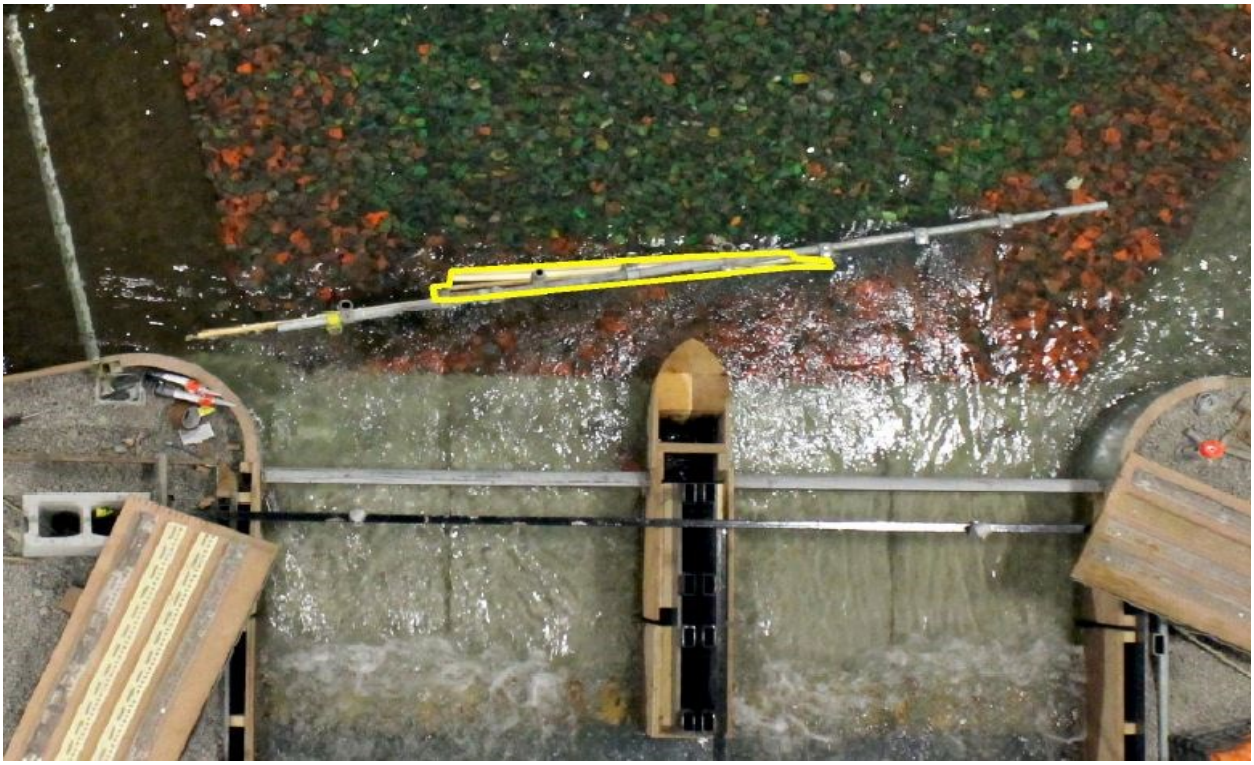

Figure 29: 10 piece dam for MD

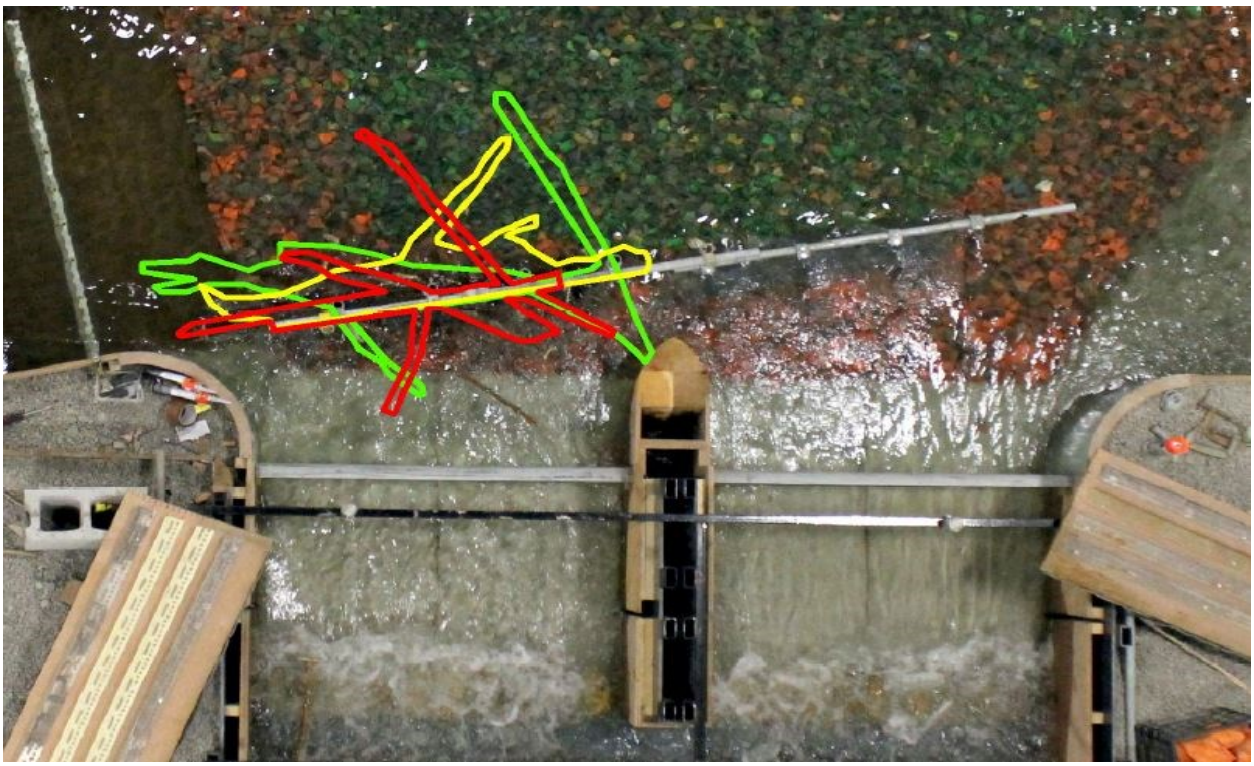

Figure 30: 9 piece dam for RDN: 1 (red), 2 (yellow), 3 (green) of 3 dams

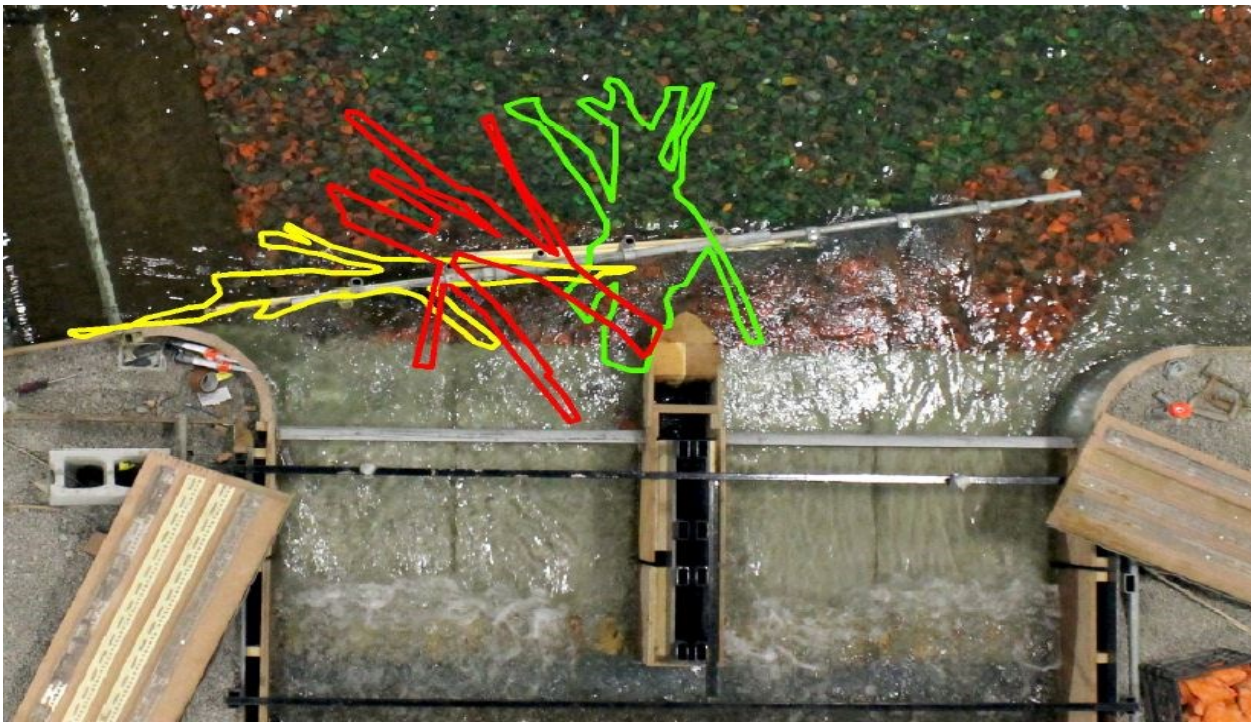

Figure 31: 10 piece dam for RDN: 1 (red), 2 (yellow), 3 (green) of 8 dams

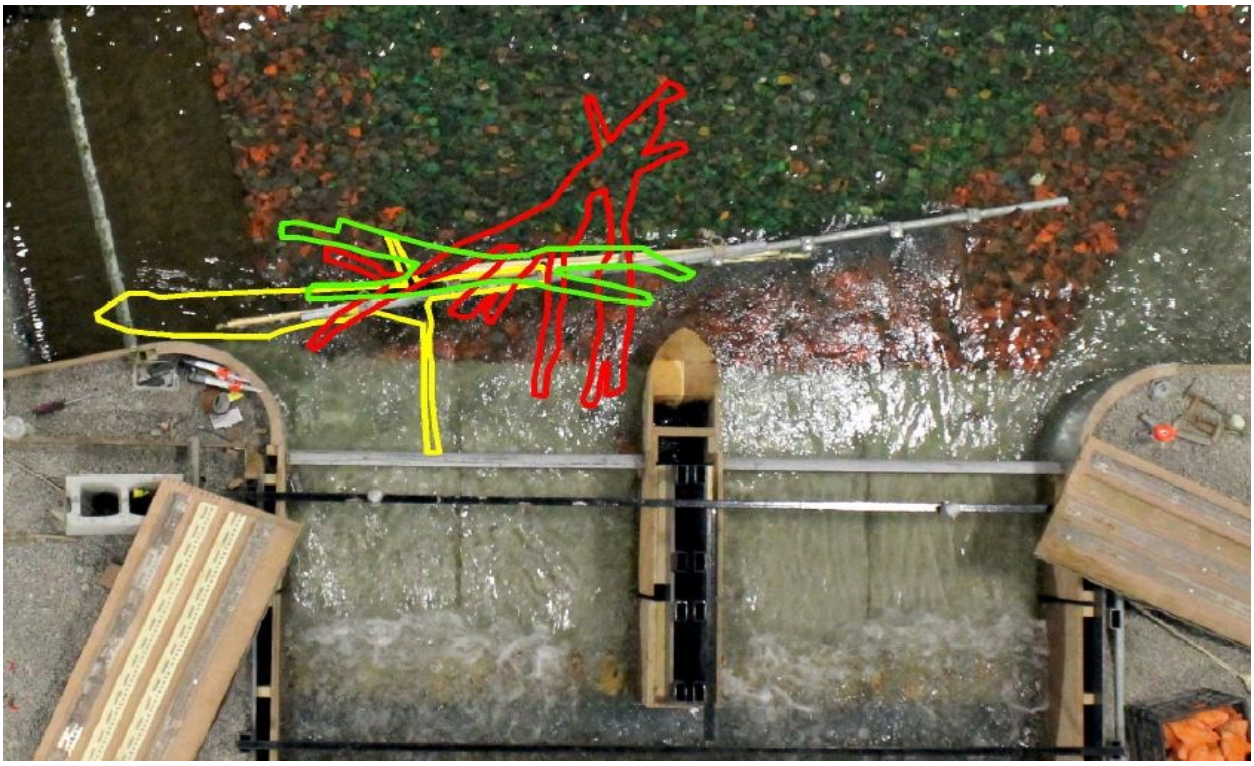

Figure 32: 10 piece dam for RDN: 4 (red), 5 (yellow), 6 (green) of 8 dams

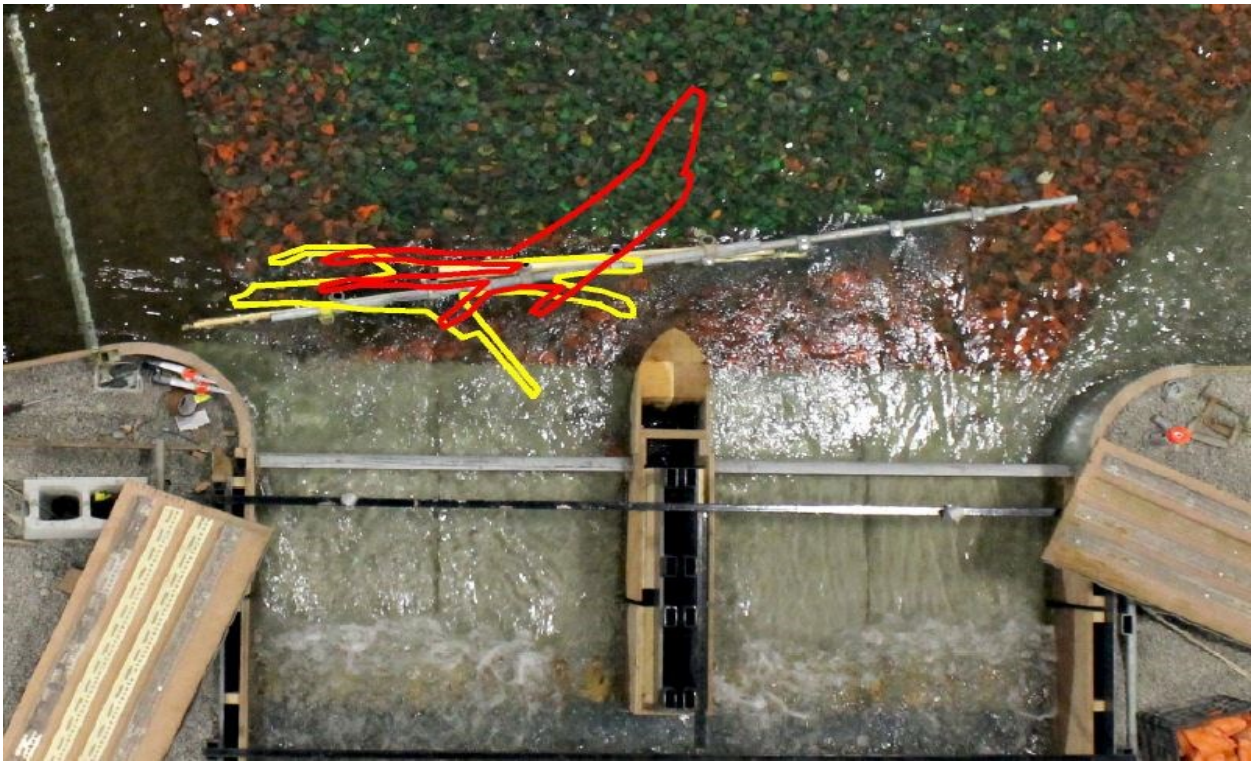

Figure 33: 10 piece dam for RDN: 7 (red), 8 (yellow) of 8 dams

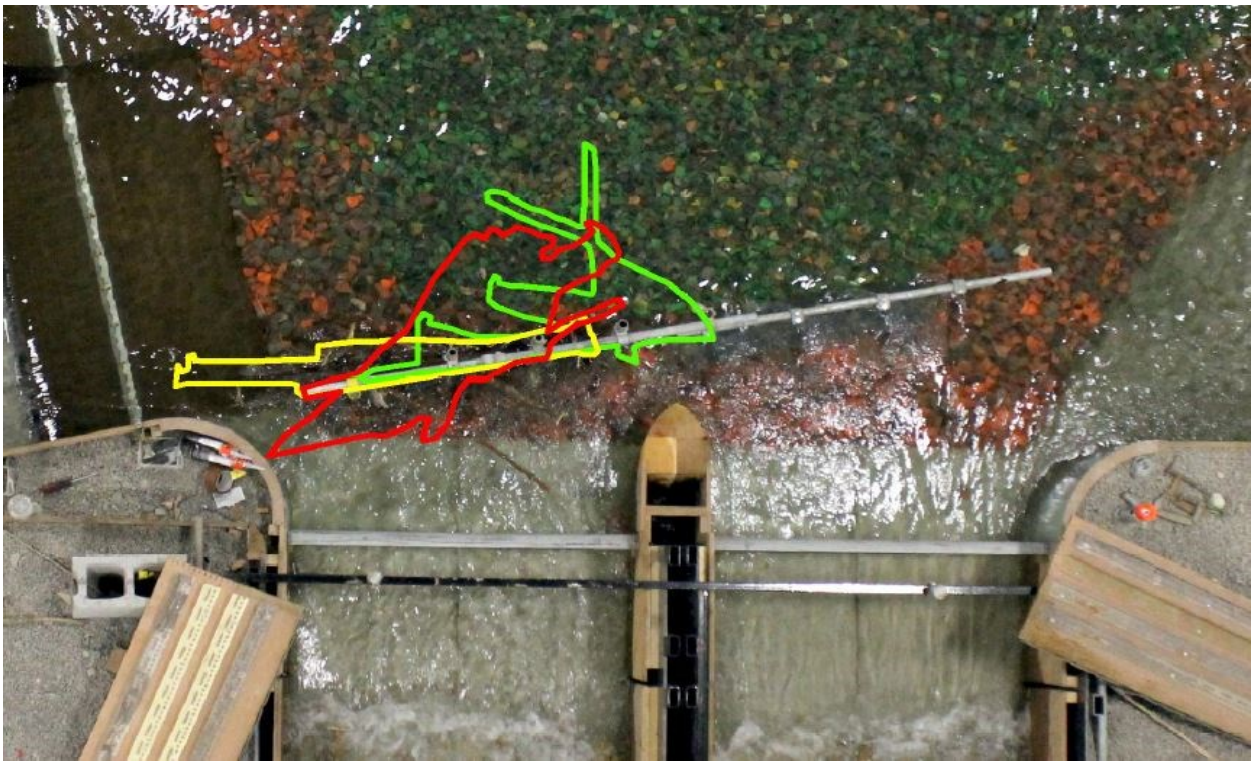

Figure 34: 9 piece dam for RDR: 1 (red), 2 (yellow), 3 (green) of 6 dams

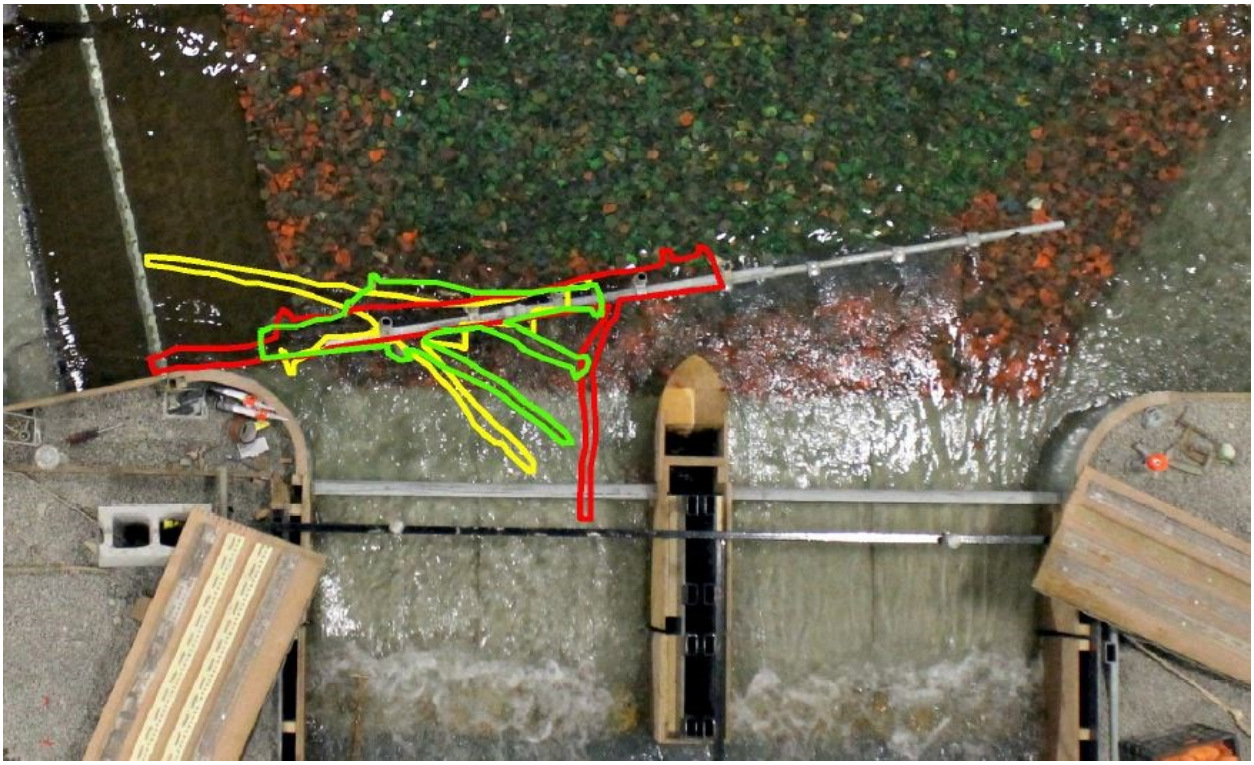

Figure 35: 9 piece dam for RDR: 4 (red), 5 (yellow), 6 (green) of 6 dams

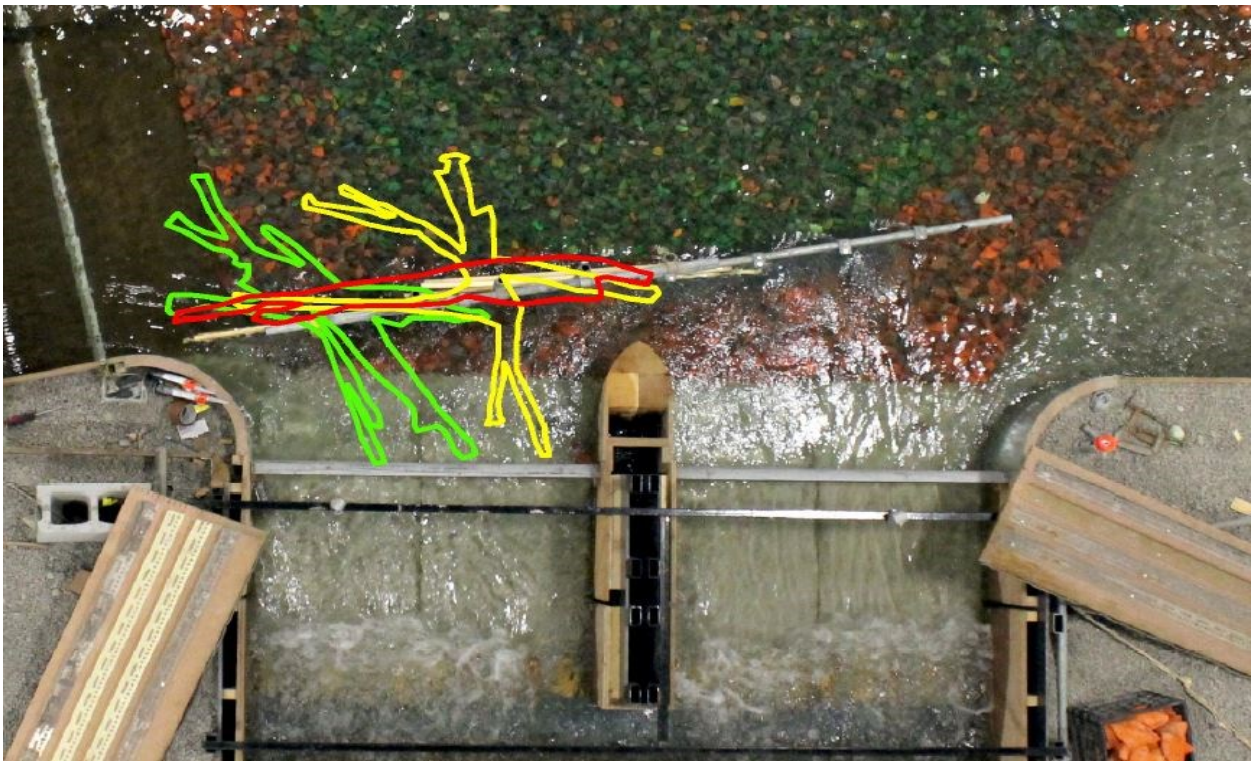

Figure 36: 10 piece dam for RDR: 1 (red), 2 (yellow), 3 (green) of 8 dams

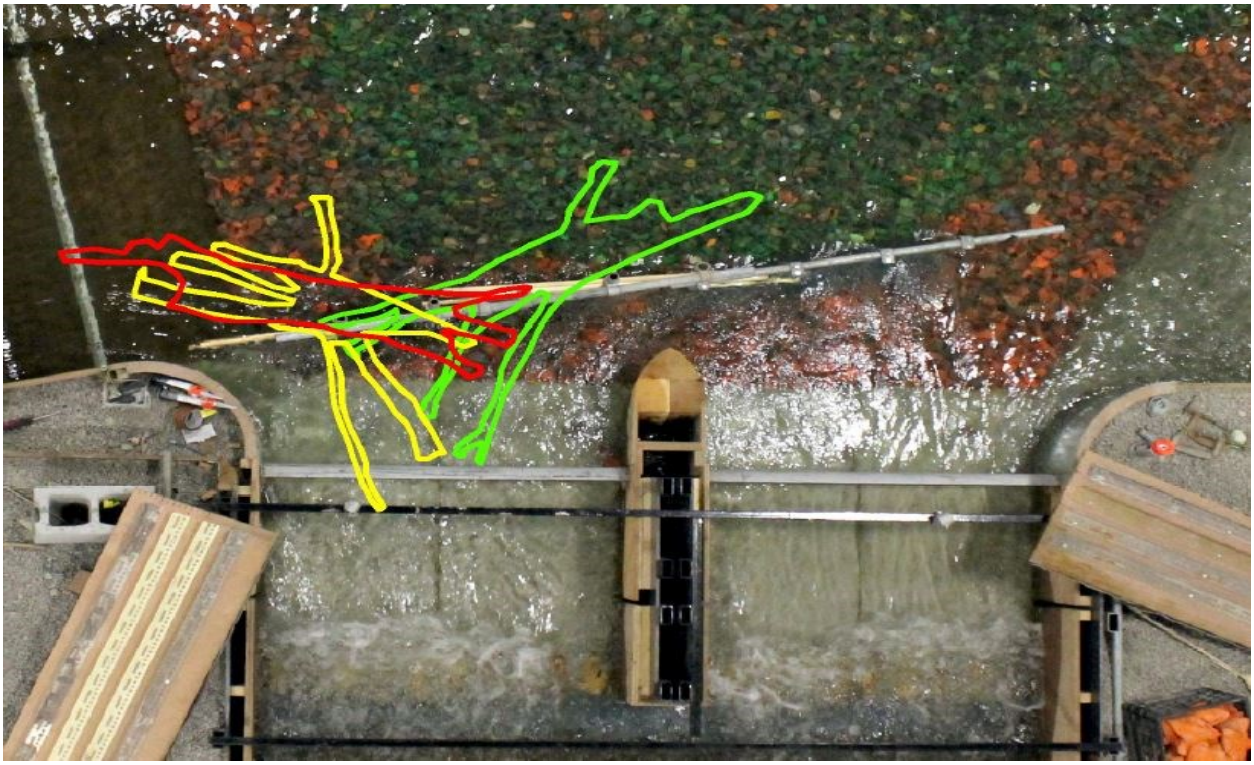

Figure 37: 10 piece dam for RDR: 4 (red), 5 (yellow), 6 (green) of 8 dams

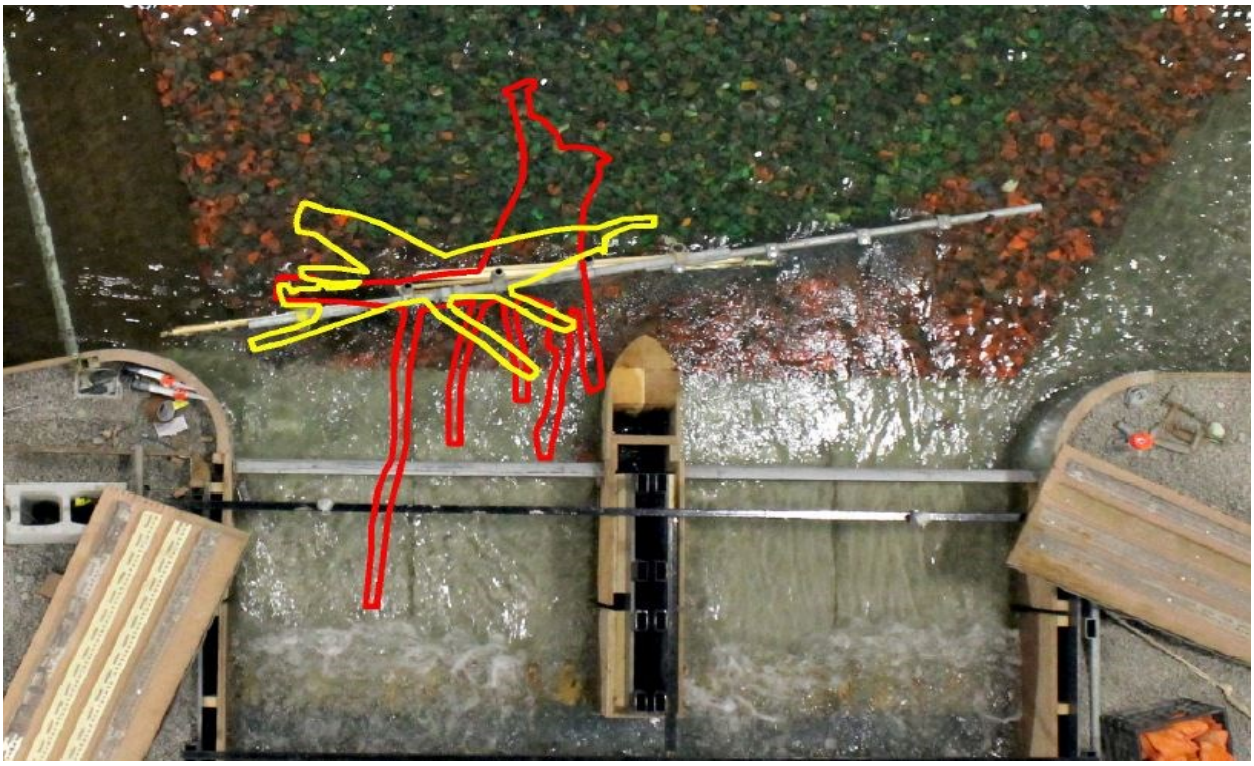

Figure 38: 10 piece dam for RDR: 7 (red), 8 (yellow) of 8 dams

Appendix B: Physical Model Construction

The physical model was constructed over the span of several months in the Large Area Basin (LAB), a rectangular basin spanning 50m by 30m and capable of depths greater than 1m. Based on bathymetric and topographic data provided to the NRC, as well as construction drawings for the flow structures, the model could be scaled down and constructed. The first step for the construction consisted of levelling in wooden pads to ensure that all templates could be easily attached to the floor of the LAB and that they were all at the same elevation. From there, ply wood templates representing the bathymetry or topography were cut using a CNC router available on the NRC campus. The templates were then installed at 1m intervals and backfilled with gravel to ensure their upright position. Figure 39 shows the templates being attached to the wooden pads and backfilled with gravel. In the background of the photo, the remaining templates needing installation can also be seen.

Figure 39: Template installation and backfilling with gravel (NRC, 2016)

Once a large portion of the templates were installed and filled with gravel, grout was ordered and brought into the LAB via concrete truck. The grout was poured onto the gravel and finished to be flush with the top of the templates. The grout was then given artificial roughness using a broom and scaled trees placed in the wet grout to simulated forested areas. Figure 40 displays the finishing process, scaled trees and concrete truck/crane used for pouring the grout.

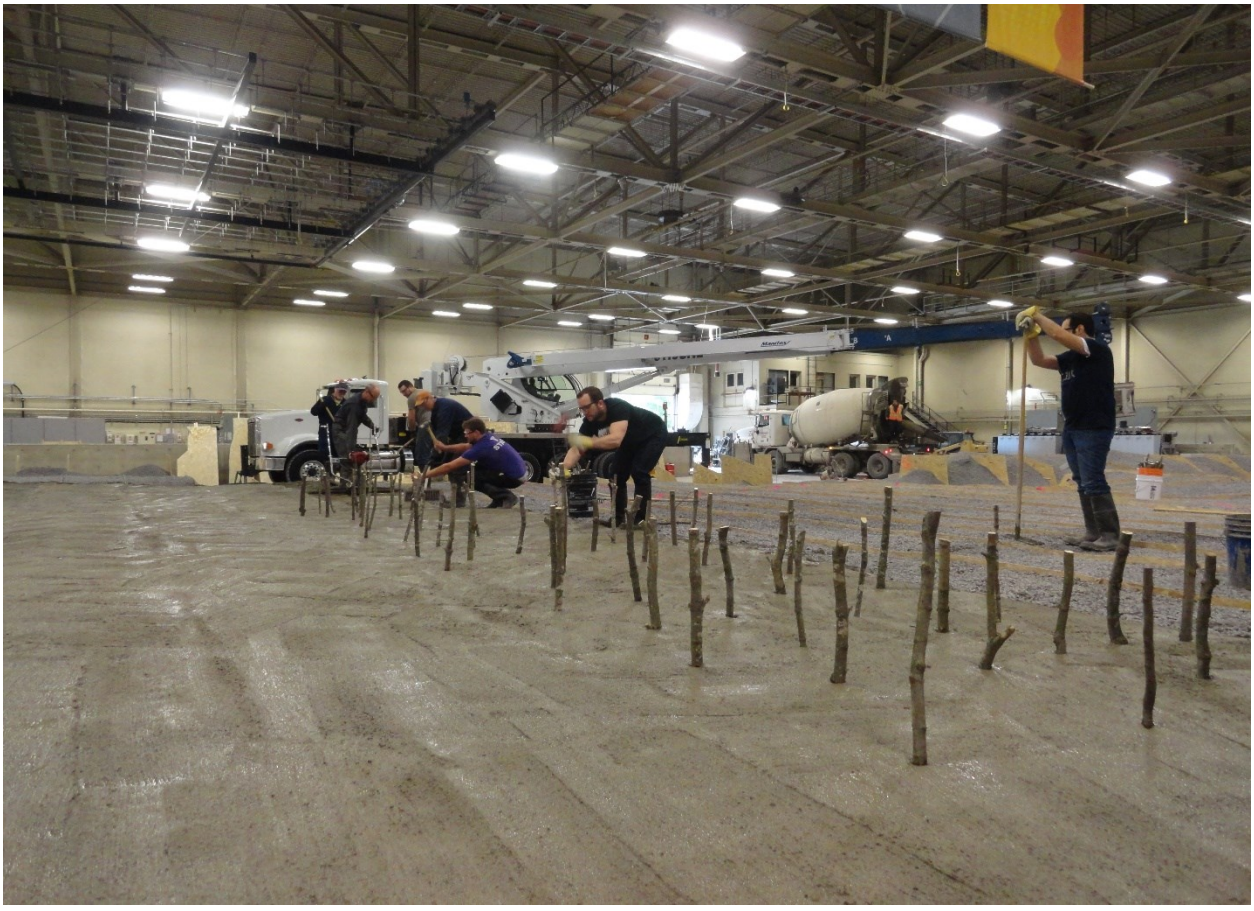

Figure 40: Grout finishing and installation of scaled trees (NRC, 2016)

This process was repeated for the entirety of the model and figure 41 provides a better perspective of the size and scale of the model that was constructed. From the photo, one can see the forested areas, the berm, and the main/secondary channels beginning to take shape.

Figure 41: Continued construction of the Springbank model (NRC, 2016)

Following the completion of the bathymetry, it was time to construct and install the flow structures. Based on the provided drawings, scaled version of the main and diversion flow structures were constructed outside of the model and then brought into the LAB for installation. Figure 42 displays the installation process for the diversion and main channel flow structures as well as the retaining walls. The majority of the main channel structure was constructed from wood due to its low cost and ease of workability. The diversion channel was mostly constructed from PVC and supports for the structures were constructed from square metal piping. The pier noses for the diversion structure were cut using a CNC router and the retaining walls were constructed from metal siding with wooden frames. Once installed, any remaining bathymetry close to the structures was finished.

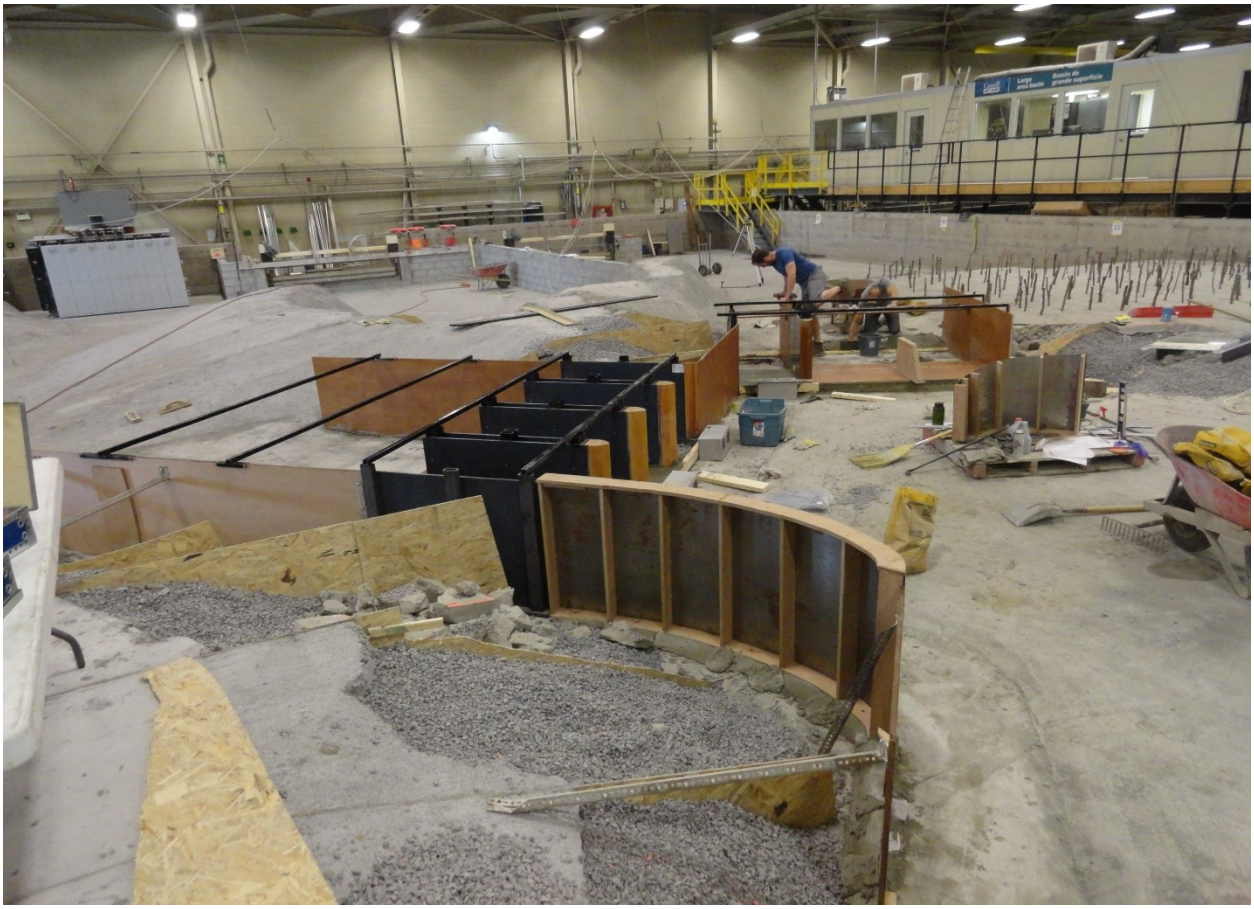

Figure 42: Installation of flow structures and retaining walls (NRC, 2016)

Following the completion of the general flow structure design, additional detailing was required to simulate exactly the design provided to the NRC. This included the addition of chute blocks on the downstream end of the diversion channel, placement of riprap in front of the main and diversion structure, and sluicegate installation for the main channel structure. Figure 43 displays these works. The riprap was spray painted in order to show any movement during testing, as the underside of the rocks would not be coloured.

Figure 43: Finished flow structures with riprap placed directly upstream (NRC, 2016)

The riprap was similarly scaled like the structures and painted two colours. Orange for the zone closest to the structures and green for the upstream area where the expected confluence would exist. The sluicegate was constructed from clear Plexiglas and the chute blocks cut from wood and installed onto wooden sheets, which were then screwed into the bathymetry. All wood in the model was finished with a sealant prior to testing in order to prevent deterioration or sagging. Figure 44 shows the completed model from the downstream perspective.

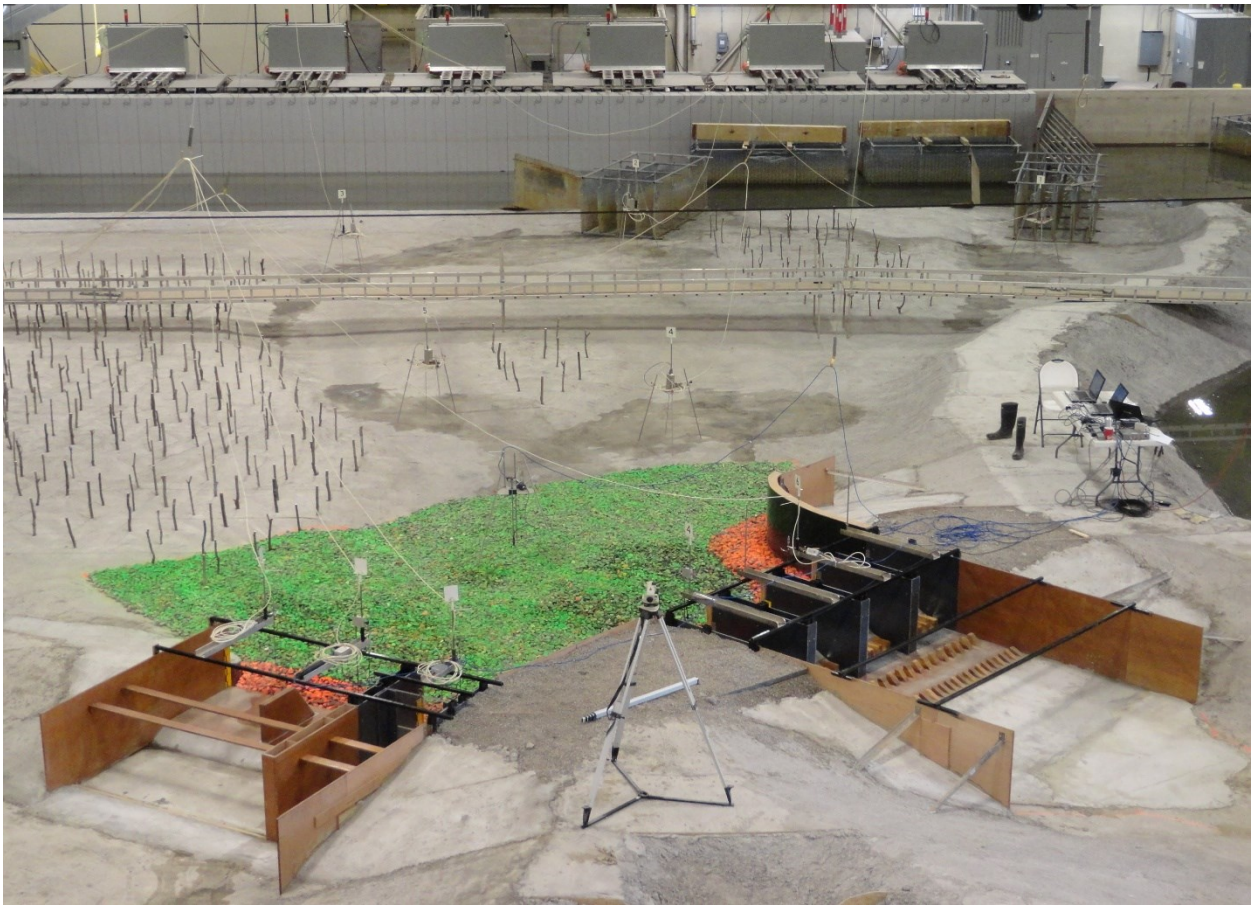

Figure 44: Completed model prior to testing with sampling equipment installed (NRC, 2016)

The wave probes and ADVs installed throughout the model were attached to wires, which hung from the rafters and ran directly into the collecting computers, which can be seen on the right side of the model. Each probe/ADV was numbered and calibrated prior to testing and were only present for clear water testing. Flow straighteners can be seen in the upstream section of the model and were installed with the hopes of reducing the impact that the flow must take to enter the model. A walkway was installed across the model for ease of access to the sampling computers.

Appendix C: Drogue Paths

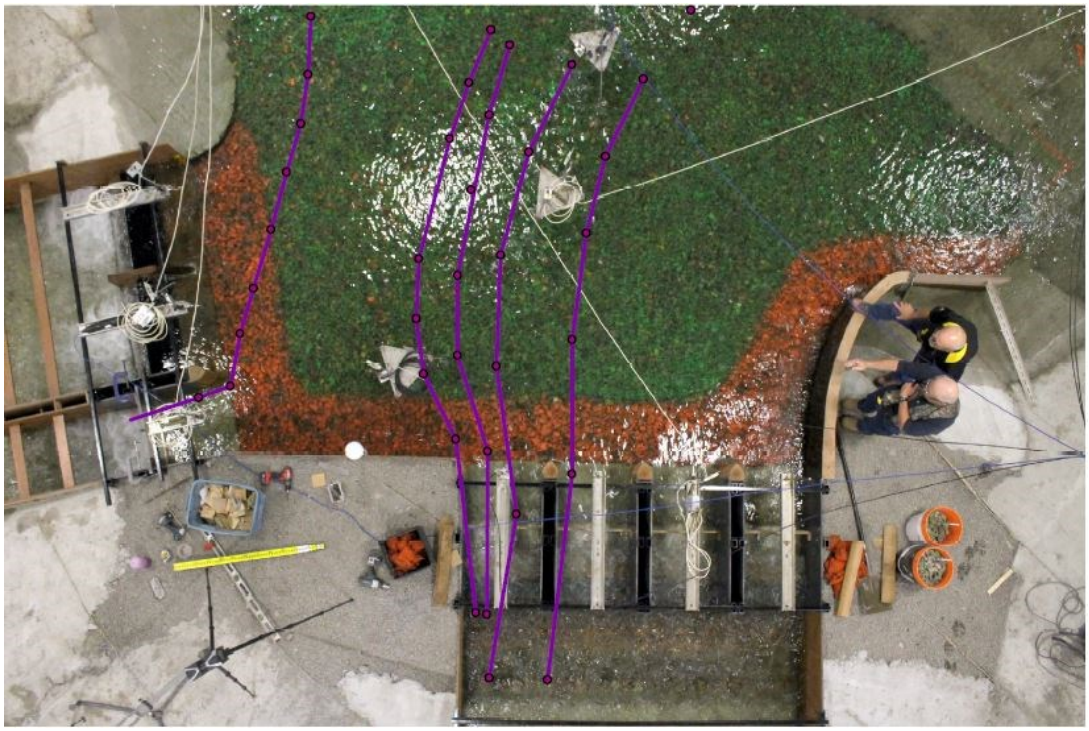

Figure 45: A_760_2: downstream drogue paths for 760m³/s flow condition

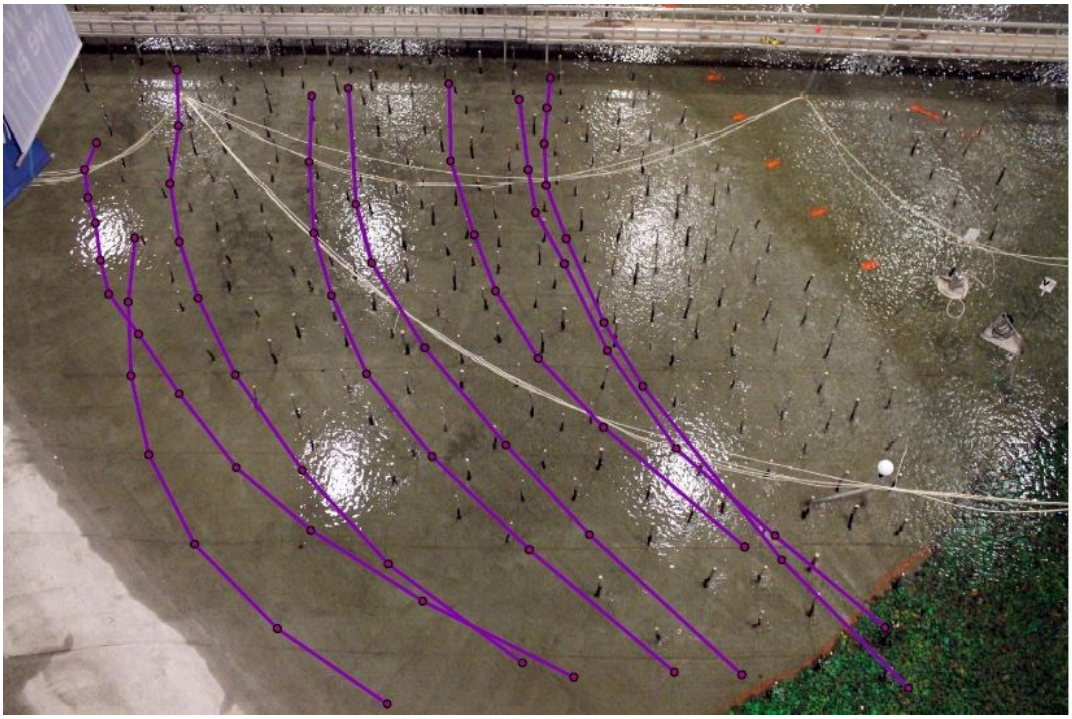

Figure 46: A_760_4: upstream drogue paths for 760m³/s flow condition

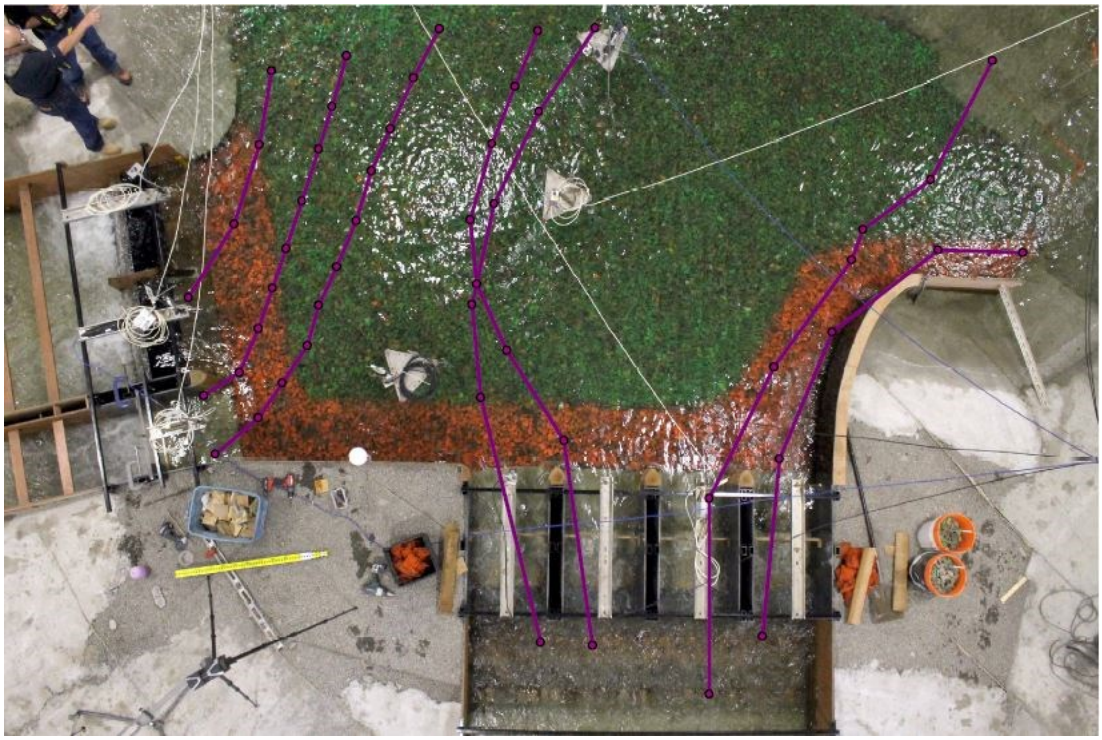

Figure 47: A_760_6: downstream drogue paths for 760m³/s flow condition

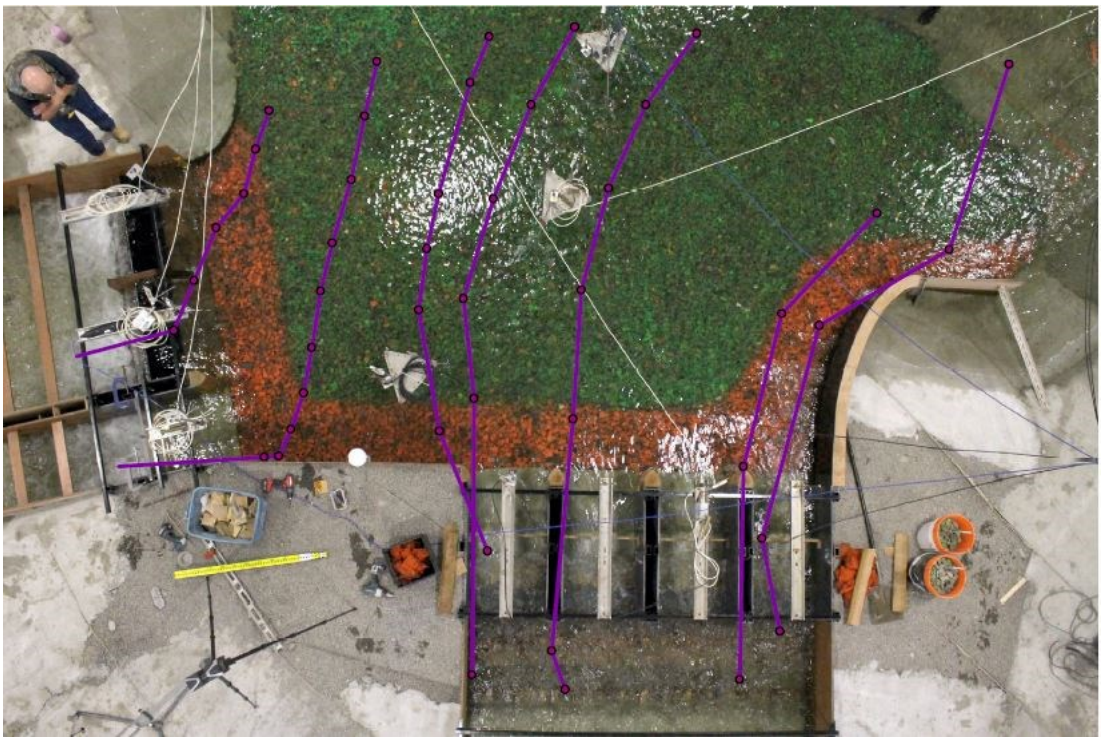

Figure 48: A_760_7: downstream drogue paths for 760m³/s flow condition